Introduction to Fluorescence Microscopy

Radek Macháň

Contents

R. Macháň (✉)
Singapore Centre for Environmental Life Sciences Engineering (SCELSE), Nanyang Technological University (NTU), Singapore, Singapore
e-mail: radek.machan@ntu.edu.sg

R. Šachl, M. Amaro (eds.), *Fluorescence Spectroscopy and Microscopy in Biology*, Springer Ser Fluoresc (2023) 20: 141–200, https://doi.org/10.1007/4243_2022_34,
Published online: 3 January 2023

Abstract Owing to its chemical specificity, high brightness, live-cell compatibility and other favourable characteristics, fluorescence is ubiquitously used as a source of contrast in biological microscopy. Fluorescence microscopes are also indispensable for many fluorescence spectroscopy techniques, such as single-molecule spectroscopy, fluorescence fluctuation spectroscopy and any form of fluorescence (micro)-spectroscopy performed in-situ in living cells and organisms. This makes fluorescence microscopy a key topic of this whole volume. This chapter aims at providing a general introduction to the topic, describing a generic fluorescence microscope and its essential components with more emphasis on objective lenses and their role in determining the resolution of microscopy images. The differences between widefield and confocal microscopes are explained and the later part of the chapter introduces briefly other variants of fluorescence microscopy and approaches to increase image resolution.

Keywords Confocal microscopy · Image resolution · Optical microscopy · Optical sectioning · Super-resolution imaging

1 Introduction

Fluorescence is one of the most commonly used sources of contrast in biological microscopy. Its uses range from the most routine assays, such as counting cells based on fluorescently labelled nuclei or counting live and dead bacteria using live/dead staining [1], to the most advanced forms of super-resolution or functional imaging [2, 3]. Fluorescence as a source of contrast in biological microscopy owes its popularity to several factors including:

1. *Chemical specificity*. Selective fluorescent labelling allows visualising the spatial distribution of specific structures or molecules of interest. Some fluorescent labels are specific to certain classes of molecules (for example DNA labelling dyes [4, 5]) or to certain types of environment (for example lipophilic dyes accumulating preferentially in non-polar environments such as lipid membranes or lipid droplets [6, 7]). Besides this type of low-level specificity there exist various labelling strategies to achieve more specific targeting. These include, for example the use of fluorescently labelled antibodies or DNA sequences, genetically encoding proteins of interest tagged either with fluorescent proteins or with specific anchor sequences for fluorescent label binding [8–10]. Last but not least, some biomolecules exhibit intrinsic fluorescence (for example

photosynthetic dyes or metabolic cofactors) and can be specifically imaged by fluorescence microscopy without the need for extrinsic labelling [11, 12]. Although indispensable in fluorescence microscopy studies, fluorophores and labelling strategies are beyond the scope of this chapter. More information on this topic can be found in chapter "Choosing Fluorescent Probes for Biology" of this volume.

2. *Multiplexing capability*. There exists a broad range of fluorophores with distinct excitation and/or emission spectra. Since signals from spectrally distinct fluorophores can be readily distinguished, it is possible to image simultaneously, or nearly simultaneously, several species of molecules or structures of interest selectively labelled by distinct fluorophores. Such images can be then used, for example, to evaluate colocalisation between different species of proteins or other biomolecules [13–15]. When linear spectral unmixing is used (see Sect. 2.2.1), even signals from fluorophores with highly overlapping spectra can be separated, allowing distinguishing of more than 100 different spectral signatures in fluorescence images [16].
3. *Environmental sensitivity*. Fluorescence brightness, spectra as well as fluorescence lifetimes of many fluorophores are sensitive to the fluorophore's environment. This allows fluorescence microscopy to image distributions of, for example, pH, polarity, viscosity, or the concentration of specific ions [17–19] inside of living cells or multicellular organisms.
4. *High brightness.* Fluorescence is typically several orders of magnitude brighter than Raman scattering, another source of chemically specific contrast in microscopy [20]. While fluorescence cannot compete with Raman scattering in the amount of chemical information it provides, its high brightness allows on one side direct observation of fluorescence in microscope eyepieces and, on the other side, it permits imaging and tracking of individual fluorophore molecules.
5. *Compatibility with living cells and organisms.* Like most other forms of optical microscopy, fluorescence microscopy is suitable for imaging living cells or multicellular organisms. Low excitation intensities are often sufficient to obtain enough fluorescence signal, resulting in low phototoxicity and making fluorescence microscopy suitable for live-cell and live-organism imaging over extended periods of time [21, 22].
6. *Technical simplicity and affordability.* In its simplest forms, fluorescence microscopy can be performed with very simple optical microscope setups, which are not fundamentally more complex than setups for brightfield optical microscopy, the simplest and oldest form of optical microscopy. Various low-cost designs of fluorescence microscopes or upgrades to brightfield microscopes have been proposed, including lens-free designs [23–32]. The technical simplicity of fluorescence microscope also ensures its straightforward combination with other optical microscopy modalities [33, 34].
7. *Super-resolution capabilities.* While in its basic forms, fluorescence microscopy offers the same resolution as other forms of optical microscopy, which means diffraction-limited at the best (see Sect. 3.1 for more details), there exist a number of techniques that allow fluorescence imaging with significantly better resolution. Most of these techniques rely on some features specific to fluorescence

microscopy such a switching of fluorophores between bright (fluorescent) and dark states or sparsity of features typical for fluorescent images. For more details, see Sect. 6 and chapter "STED and RESOLFT Fluorescence Nanoscopy".

So far, when talking about fluorescence as a source of contrast in microscopy, we have mainly considered fluorescence intensity as the source of contrast. Fluorescence intensity images inform us mainly about the spatial distribution of fluorescent probes and fluorescently labelled molecules of interest in the specimen and can be acquired even with the simplest forms of fluorescence microscopes. However, other characteristics of fluorescence can be also used to generate contrast in fluorescence microscopy and to provide different types of information about the system under study. As examples we can mention fluorescence lifetime used in fluorescence lifetime imaging microscopy (FLIM) (see chapter "Time-Resolved and Polarized Spectroscopy" for more details), fluorescence anisotropy [35, 36], fluorescence linear dichroism [37] or statistics of fluorescence intensity fluctuations employed in fluorescence correlation spectroscopy (FCS) imaging (see chapter "2D FCS Including Imaging FCS and Scanning FCS").

The term microscopy is usually associated with imaging of microstructures. However, fluorescence microscopes are also frequently used in non-imaging techniques as a device to generate small, well-defined detection volumes essential in FCS (see chapter "FCS and FCCS Principles and Applications") and other single-molecule fluorescence spectroscopies. While these techniques are often not generating images themselves, they frequently benefit from the imaging capabilities of fluorescence microscopes for positioning the detection volumes into specific regions of the specimen. This aspect has become more important as biomolecular studies move from in-vitro settings to measurements performed directly in living cells and organisms. Overall, these fluorescence spectroscopic or micro-spectroscopic techniques can be seen as a form of fluorescence microscopy in a broader sense, bringing us to the conclusion that this whole volume is dedicated largely to fluorescence microscopy. As many of more specialised modalities of fluorescence microscopy are, therefore, discussed in other chapters, this chapter limits itself only to general basics of fluorescence microscopy.

2 Epifluorescence Microscope

The most common architecture of a fluorescence microscope is an epifluorescence microscope, which employs episcopic, or in other words reflected light, mode of observation. In practice this means that the excitation light is delivered to the specimen by the same objective lens which is used for collecting the fluorescence light. A generic (widefield) epifluorescence microscope is schematically depicted in Fig. 1. An epifluorescence microscope can be built in an upright (the objective is above the specimen) as well as in an inverted configuration (the objective is below the specimen), whichever configuration is more suitable for the specimens of

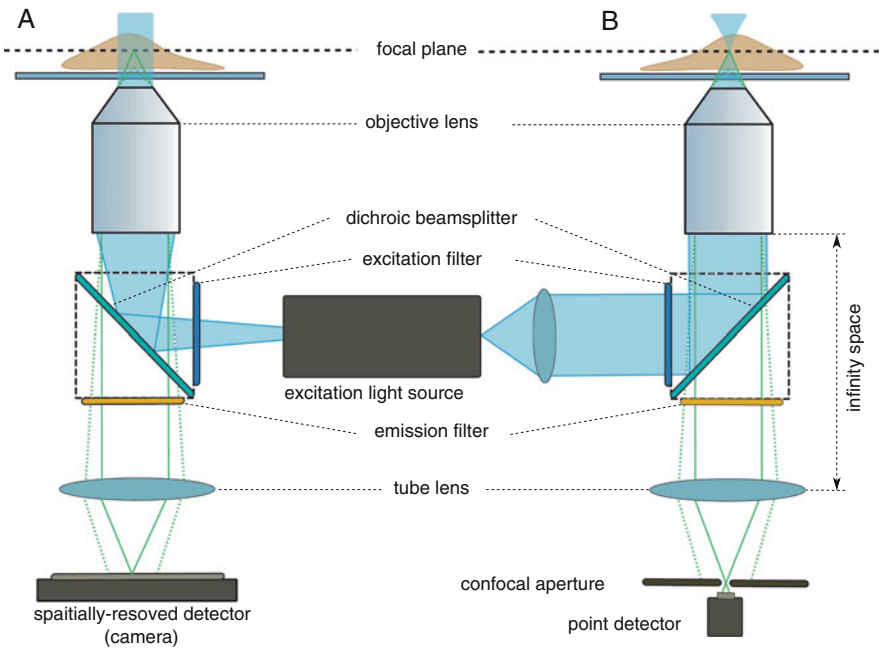

Fig. 1 A schematic drawing of the main components of an inverted widefield (**a**) and confocal (**b**) epifluorescence microscope. Refer to Sects. 2.1–2.4 for an explanation of the role of the individual components. Green lines schematically illustrate rays of fluorescence emitted from an in-focus fluorophore (solid lines) and an out-of-focus fluorophore (dotted lines). The rays from the in-focus fluorophore are focused in the primary image plane producing a sharp (diffraction limited) image of the fluorophore, while the unfocused rays from the out-of-focus fluorophore produce a blurry background. Confocal aperture in the confocal setup (**b**) stops most of the out-of-focus fluorescence from reaching the detector (see Sect. 4 for more details)

interest. The inverted configuration is preferred for imaging cells in culture dishes and similar systems, where small objects are found close to the bottom of a dish filled with a liquid medium. The upright configuration is more convenient for imaging larger non-transparent objects, for example intravital imaging in rodents. Microscope slides are easily imaged in either configuration. The schematic in Fig. 1 shows explicitly an inverted microscope; turning the figure by 180° gives a schematic of an upright microscope.

2.1 Light Sources

The excitation light in an epifluorescence microscope can be provided by lasers or incoherent light sources, often referred to as lamps. Lasers are used in confocal microscopy (see Sect. 4), while incoherent light sources are common in widefield fluorescence microscopy with the exception of some specialised widefield

modalities such as total internal reflection fluorescence (TIRF) microscopy (see Sect. 5.3). Mercury or Xenon arc lamps producing white light covering a broad spectral range from ultraviolet (UV) to near infrared (NIR) used to be the most common light sources in widefield epifluorescence microscopy. Mercury metal halide lamps offered a similar spectrum with the advantages of a longer lifetime and easier operation. However, all these lamps have been largely rendered obsolete by solid-state light sources usually based on light-emitting diodes (LEDs). LEDs often emit in relatively narrow spectral ranges (although white-light LEDs are also available); therefore, LED-based light sources usually contain several LEDs which together cover the whole desired spectral range. Their advantages include very long lifetimes, high-intensity stability, high energy efficiency [38, 39] as well as fast modulation capabilities [40]. Beside the high efficiency of conversion of electric energy to light, solid-state light sources have three additional advantages which contribute to the overall energy efficiency of the microscope:

1. LEDs can be switched on and off nearly instantaneously. Therefore, they can be on only when excitation light is needed. In contrast, metal halide or arc lamps have quite long warm-up times and cannot be switched off, for example, between the acquisition of individual images; a mechanical shutter has to be used instead to prevent the excitation light from reaching the specimen when it is not needed.
2. The output power of LEDs can be regulated electronically, hence they do not need to emit at full power if only low excitation light intensity is required. Neutral density filters or aperture stops are used to control the excitation light intensity produced by metal halide or arc lamps, while the lamp itself emits at its full power.
3. Only a narrow spectral band of excitation light is usually used at a time to specifically excite certain fluorophores of interest. Since metal halide or arc lamps produce white light covering a broad spectrum, the desired spectral band is selected by an excitation filter (see Sect. 2.2.) which blocks the rest of the light from reaching the specimen. Most of the output of the lamp is, thus, typically wasted. On the other hand, since solid-state light sources usually contain multiple LEDs, each emitting only in a relatively narrow spectral band, only the LED emitting in the desired spectral band can be turned on.

The combination of nearly instantaneous on and off switching and narrow spectral bands (see points 1 and 3 above) makes LED-based light sources well suited for very fast multi-channel fluorescence imaging. Rapid switching between different excitation spectral bands, without the need for any mechanically moving parts, enables nearly simultaneous selective excitation of different fluorophore species in the specimen. To fully benefit from the high speed of excitation band switching, there must be no other mechanical movements involved in switching between different fluorophore channels; the microscope, therefore, needs to be equipped with a main beamsplitter and an emission filter that is suitable for all the fluorophores of interest (such as a polychroic mirror or a partially reflective mirror and a multi-band emission filter; see Sect. 2.2 for more details).

2.2 Beamsplitters and Filters

Light from an excitation light source (see Sect. 2.1) passes through an excitation filter to select the desired excitation spectral window. Excitation filters are not needed if the light source emits only in a narrow spectral band such as is the case with most lasers and some LEDs. In setups with multiple laser lines available for excitation, acousto-optical tuneable filters are sometimes employed instead of excitation filters to select a desired laser line or a combination of lines. Together with the ability of rapidly switching the excitation laser lines, they offer an additional capability of fast modulation of a laser line intensity [41].

The excitation light is then reflected by a beam splitter, the main or primary beam splitter, to the microscope objective. Fluorescence emitted by the specimen is collected by the same objective and passes through the primary beam splitter in order to reach the detection device, for example a digital camera or human eye. The primary beam splitter thus plays the key role of separating the excitation and emission light paths. It is usually a dichroic mirror which reflects light of wavelengths shorter than a cut-off wavelength and transmits light of longer wavelength. The separation is, therefore, based on the well-known phenomenon of Stokes shift, the red shift of a fluorophore's emission spectrum compared to its excitation spectrum. It is a very efficient way of separating the emission and excitation paths since the losses of emission as well as excitation light are minimal on a properly chosen dichroic mirror. The disadvantage of a dichroic mirror with a single cut-off wavelength is its limitation to a specific spectral window. When a specimen labelled by multiple, spectrally distinct fluorophores needs to be imaged, a different dichroic mirror has to be used for each fluorophore, which slows down the acquisition speed. This limitation is overcome by polychroic mirrors, which have several alternating reflection and transmission bands. They allow simultaneous or nearly simultaneous (for example with a light source allowing very fast switching of excitation spectral bands; see Sect. 2.1) excitation of distinct fluorophore species. Polychroic mirrors with 2 to 4 bands are commonly used in fluorescence microscopy and mirrors with higher numbers of bands are also available. With increasing number of spectral bands, the transmissive spectral windows have to be narrower, which reduces the amount of fluorescence light that can reach the detection device. The loss in fluorescence signal tends to be more prominent for fluorophores with broader spectra that are more likely to stretch further over the other reflective spectral bands.

Where full flexibility in the choice of excitation wavelengths and their combinations is important, an acousto-optical beam splitter can be used as the primary beam splitter [42]. The device acts as a polychroic mirror with arbitrarily tuneable reflection and transmission bands. The drawbacks are the increased cost and complexity of such a setup. Alternatively, a broad-band partially reflective mirror (for example with 10% reflectivity and 90% transmissivity across the whole visible spectrum) can be used as a low-cost alternative in such cases. Similarly to an acousto-optical beam splitters, it is suitable for any combination of excitation and emission bands. Its low efficiency in delivering excitation light to the objective can be compensated by

increasing the excitation light source power. If the excitation source is powerful enough, even lower reflectivity to transmissibility ratios can be used to minimise the loss of fluorescence light on the beamsplitter. A limitation lies in its lack of spectral selectivity. Reflected or back-scattered excitation light passes the mirror equally well as fluorescence and all the burden of blocking the unwanted excitation light then falls on the element which typically follows after the primary beam splitter – an emission filter.

The role of the emission filter is to block unwanted reflected and scattered excitation light from reaching the detection device and to define the spectral band in which fluorescence is detected. It, therefore, increases the specificity of detecting the fluorescence signal of interest. Similarly to dichroic and polychroic mirrors, there exists a range of long-pass, single band-pass and multiple band-pass filters. Fluorescence spectra are usually quite broad, spanning ranges often exceeding 100 nm; therefore, compromises are usually needed between the requirements of specificity (enhanced by narrow-band filters) and maximising collected signal (increasing with broader transmissivity bands of the filters). When we want to specifically image individual fluorophore species in a specimen labelled by multiple fluorophore species, selective excitation of individual species by light of appropriately selected wavelengths applied one at a time is usually more efficient and preferred compared to attempting emission signal separation by narrowing down the emission filter transmission bands. When multiple fluorophore species are excited by the same wavelength, it is often impossible to detect the signal from an individual fluorophore species only, without contamination with signal from the other simultaneously excited species (so-called spectral crosstalk). Linear spectral unmixing introduced in Sect. 2.2.1 may be necessary in such a case to separate contributions from the individual fluorophore species.

Matched sets including an excitation filter, a dichroic or polychroic mirror and an emission filter, for a certain spectral range of fluorescence, are commonly mounted in filter cubes. The whole filter cubes are then exchanged when switching between fluorophores, either by rotating a filter cube turret or translating a filter cube slider. In some setups, excitation filters, beam splitters and emission filters are mounted in separate turrets and can be thus freely combined. This flexible arrangement is advantageous when two fluorophores (or a single environmental sensitive probe in two different environments) excited by the same wavelength but emitting at different spectral windows, which means exhibiting different Stokes shifts, are present in the specimen. A single excitation filter and dichroic mirror alongside with two different emission filters are sufficient in this case. An example is probing lipid membrane organisation with Laurdan, which changes its emission spectrum in response to the membrane phase [43].

In some cases, for example when the process under study is very fast, it is necessary to capture the signal from multiple fluorophores truly simultaneously. Polychroic mirrors as main beam splitters can help in such cases by enabling simultaneous excitation in different spectral bands; however, a single multi-band emission filter and a single-detection device are not sufficient in this case since they would not allow separation of the signals from individual fluorophores. Multiple

detection devices are needed, each collecting light in a different spectral window. Secondary dichroic beam splitters and emission filters are then usually employed to spectrally separate the fluorescence signals. The individual detection devices can be, for example separate digital cameras or separate portions of the chip of a single camera. The latter approach, beside reducing the cost of the setup by decreasing the number of cameras needed, is advantageous in situations where the final experiment output is sensitive to camera noise characteristics, such as in fluorescence fluctuation spectroscopies [44]. Its obvious limitation is a reduction of the accessible field of view.

The choice of beam splitters and filters is an important step in a fluorescence microscopy experiment design. The choice is based on the excitation and emission spectra of fluorophores used to label the specimen, with the goals of maximising the portion of the emission spectrum detected and, in the cases when multiple fluorophore species are used, of minimising the spectral crosstalk between individual spectral channels. Fluorophore spectra databases are a useful tool for this task [45]. Note that matching the detection spectral window to the emission spectrum of a fluorophore is more important than matching the excitation wavelength to the fluorophore's excitation spectrum maximum. The reduced excitation efficiency, when using a wavelength outside of the excitation spectrum maximum, can be compensated by increased excitation light intensity. Light which is not absorbed by the specimen is not likely to cause it any harm. Therefore, if the excitation light is not strongly absorbed by other molecules in the specimen than the fluorophores of interest, the risk of photodamage and phototoxicity scales with the excitation rate of the fluorophores rather than the excitation light intensity itself. On the other hand, there are no easy ways to compensate for fluorescence light lost on sub-optimally chosen filters or beam splitters, other than, for example, extending image integration times (and thus the duration of the experiment), detection gain (and thus the noise in the image) or fluorophore excitation rate (and thus the risk of increased fluorophore bleaching and photodamage of the specimen).

Spectral crosstalk is minimised by selecting fluorophores with spectrally well-separated emission and/or excitation. However, the more different fluorescent labels are present in the specimen, the smaller the spectral separation between them can be, eventually leading to the presence of fluorophores with overlapping spectra. In such cases, dichroic mirrors and optical filters are not sufficient to unambiguously separate signals from such fluorescent labels. Linear spectral unmixing can be a solution to this problem.

2.2.1 Linear Spectral Unmixing

We assume that the fluorescence emission spectrum of a mixture of fluorophore species is a linear combination of emission spectra of the individual species weighted by the relative abundance of each fluorophore species. If we acquire a multi-channel image with C fluorescence channels, then in each pixel of the image, we get the following intensities in each channel:

$$I_c = \sum_{s=1}^{S} M_{cs}\, w_s$$

Index c denotes the fluorescence channel and goes from 1 to C, index s identifies the fluorophore species and goes from 1 to S, the number of the fluorophore species. w_s is the weight with which s-th fluorophore species contributes to the overall signal, or in other words, the relative abundance of the s-th fluorophore in the mixture. M_{cs} are the elements of the so-called mixing matrix which describes the contribution of each fluorophore species to the individual channels, that means their normalised spectral signatures. The mixing matrix can be found by acquiring images (with the same set of C channels) in samples containing each a single fluorophore species only.

By measuring the signal in all C channels, we obtain a set of C equations for S unknown weights w_s. This set of equations can be unambiguously solved only when C is larger than or equal to S. This means we need at least as many channels as we have fluorophore species. The unknown weights w_s are then obtained from the following equations:

$$w_s = \sum_{c=1}^{C} U_{sc}\, I_c$$

U_{sc} are the elements of the unmixing matrix, which can be found by matrix inversion (in the case when $C = S$) or pseudo-inversion (when $C > S$) of the mixing matrix. Finding the weights w_s for all pixels in the image gives us a new multi-channel image of S channels, each channel corresponding to the distribution of a single fluorophore species.

When spectra of two fluorophore species, i-th and j-th, are heavily overlapped, the corresponding mixing matrix elements M_{ci} and M_{cj} are likely very similar for all channels c, compromising the reliability of the unmixed weights w_i and w_j. Increasing the number of channels C may help in such cases by leveraging subtler difference in the fluorophore spectra. On the other hand, higher number of channels C implies narrower spectral bands for each channel, resulting in lower signal in each channel and, therefore, in compromised signal-to-noise ratio. Lower signal-to-noise ratio is another factor increasing the uncertainty in the unmixed weights.

Because we have assumed a linear mixing model, where the spectrum of a mixture of fluorophore species is a linear combination of spectra of the individual species, linear spectral unmixing fails where this assumption is not met. This is, for example the case of saturated pixels. If the pixel value in a channel exceeds the dynamic range of the image, the value is clipped at maximum of the dynamic range. This affects the ratios between intensities I_c in different channels and leads to incorrect weights w_s. The more a fluorophore species contributes to the saturated channel, the more will its weight be underestimated.

In some cases, the mixing matrix M_{cs} is not known. For example, when working with a sample exhibiting multiple spectral patterns of autofluorescence, it is not

possible to measure spectra of each autofluorescence component separately. For such situations, various blind spectral unmixing algorithms have been proposed, which estimate spectral signatures of the individual fluorophore species based on the distribution of mixed spectra present in individual pixels of the image [46, 47].

2.3 Image Formation

So far, we have not touched on the image-forming optics, which form the core of any optical microscope. As mentioned earlier, in epifluorescence microscopy, the objective lens has the double role of delivering excitation light to the specimen and of imaging the emitted fluorescence. Modern optical microscopes use the so-called infinity-corrected optical system. In this system, the objective lens, called infinity-corrected objective lens, is not used alone to produce the magnified image. Instead, it collimates rays originating from the focal plane. The collimated, that means parallel, rays are then focused by another lens, called tube lens, to produce a magnified image. Optical filters and beamsplitters are typically located in the so-called infinity space between the objective lens and the tube lens. Since the fluorescence light is collimated in this space, plan parallel optical elements such as optical filters do not disturb its wavefront. The image formed by the tube lens, called the primary image, can be then viewed by the microscope eyepiece or captured by a spatially resolved detector such as a digital camera, with its sensor positioned in the primary image plane. In some setups, though, the image formed by the tube lens is relayed to the camera sensor by a telescope (a pair of lenses) to increase or decrease the magnification of the image or to gain space for other optical elements such as secondary beamsplitters and filters.

Objective lenses are critical in determining the quality and resolution of microscopy images. Because of its central importance, the whole Sect. 3 is dedicated to this topic.

2.4 (Widefield) Image Detection

The last component in the detection optical path is the detection device itself. As we said above, in widefield epifluorescence microscopy, it is usually a spatially resolved sensor, or in other words a digital camera. Such a sensor is a two-dimensional array of small photosensitive elements, which we can call the physical pixels of the sensor, or pixels for short in the context of this section which is dedicated to camera sensors. In other context the term pixel can also refer to image pixels, the unit building blocks of a digital image. While those two are clearly linked (typically the intensity values of image pixels are proportional to the signal detected by the camera physical pixels), there is a conceptual distinction between them.

For fluorescence microscopy, monochrome cameras are usually preferred because of their higher sensitivity. A typical colour camera sensor contains pixel-level colour filters that make different physical pixels sensitive to light of different colour. In the usual Bayer pattern, in a group of 4 (2 × 2) neighbouring physical pixels, one is sensitive to blue light, one to red light and two are sensitive to green light [48]. Since the spectral bands for fluorescence detection are typically defined by the emission filters, the spectral information provided by a colour camera is redundant and the pixel-level colour filters only lead to additional signal losses. Furthermore, red or blue fluorescence is detected only by a fourth of the physical pixels (1 pixel in each group of 4), resulting in a correspondingly reduced sensitivity in that part of the spectrum.

The first digital camera technology that become widespread in fluorescence microscopy were charge-coupled devices (CCDs). A CCD sensor is an array of metal-oxide-semiconductor (MOS) capacitors that are charged by photoelectric effect when exposed to light. These capacitors form the physical pixels of the sensor and their pitch in the array is the physical pixel size. The charges are then converted to voltage by a charge amplifier and the voltage is then digitised. A usual CCD uses a single charge amplifier for the whole chip, which means that the charges from all pixels need to be transferred to a single readout point. This is achieved by applying external voltage, which induces the charges to hop to a neighbouring pixel. Charges from whole lines of pixels are transferred in this way to the neighbouring lines. The line on the edge of the sensor area is transferred to a readout register in which the charges are moved towards the charge amplifier in a direction perpendicular to the line transfer direction. Once the charges from all pixels in the readout register have been read one by one, all lines are again shifted by one step, and a new line enters the readout register. This is repeated until each line has been read in the readout register. The process can be quite time-consuming for sensors with large pixel numbers and, unless a mechanical shutter is used, may result in image smearing caused by exposing the camera while the lines of pixels are being shifted towards the readout register. To avoid the need for a mechanical shutter, different CCD architectures with masked pixels have been developed. An interline CCD uses a sensor chip with every second row of pixels covered by an opaque metal mask. The charge accumulated in the active, non-masked, rows of pixels is transferred to the masked rows and then shifted to the readout register and read out while the next frame is being collected by the active rows. The disadvantage is the reduction of the sensor fill-factor to 50%. This can be partially compensated by the use of micro-lens arrays that focus the light to pixels in the active rows. In a frame transfer CCD, half of the sensor chip is covered by an opaque metal mask. The lines are quickly transferred to the masked area and then read out through the readout register while the next frame is being collected in the non-masked part of the sensor. This design ensures full fill-factor of the sensor at the cost of using a chip of twice the size. As such it is preferred in low-light applications, where high sensitivity is more important than low cost.

Among the advantages of CCDs are high quantum efficiency (QE, the fraction of incident photons contributing to charge generation), which can reach values above 90% and high uniformity of pixel noise characteristics ensured by using a single charge amplifier for all pixels [49, 50].

A modification of CCD sensor called electron-multiplying CCD (EM-CCD) was developed to increase the signal at very low-light levels. An amplification register, through which the charges pass on their way to readout, is added to the chip. High voltage is used to shift electrons in this register resulting in impact ionisation similarly to what happens in an avalanche photodiode. The higher the applied voltage in the amplification register, the larger the gain in electron number. Although the amplification is an additional source of noise, the large gain in signal it provides leads to significant improvements in signal-to-noise ratio at low-light levels. EM-CCDs thus became the sensors of choice for single-molecule fluorescence, calcium imaging and other low-light applications [51–54].

An alternative digital camera technology, which has become increasingly widespread in fluorescence microscopy, is complementary metal-oxide-semiconductor (CMOS) sensors. Their principal difference from CCDs lies in the fact that in a CMOS sensor, each pixel is equipped with its own charge amplifier. This makes charge readout from CMOS sensors faster than from CCDs; however, it also means that part of the sensor active area is lost to charge amplifier transistors. This problem can be partially solved by micro-lens arrays focusing light to the active area of each pixel. Another potential problem associated with pixel-wise readout is the non-uniformity in amplification and in noise caused by variations between the amplifiers at individual pixels. This used to limit the spread of CMOS sensors in scientific applications until the arrival of so-called scientific-grade CMOS (sCMOS) sensors, which feature low readout noise and high quantum efficiencies that do not lag behind CCDs. Another important development in CMOS sensor technology was the integration of field-programmable gate arrays which can be programmed to correct for sensor-specific pixel-to-pixel variations (such as so-called hot pixels or fixed-pattern noise) caused by non-uniform performance of the individual amplifiers [50, 55]. All these developments have made current CMOS sensors a viable alternative to CCDs and EM-CCDs. Being easier and cheaper to manufacture, especially at large formats, cameras with CMOS sensors have become the mainstream choice in fluorescence microscopy, pushing CCDs and EM-CCDs to the position of a niche technology reserved for highly specialised applications. sCMOS sensors are successfully used in single-molecule fluorescence and even low-cost industrial CMOS cameras or cell phone CMOS cameras have been shown to be capable of single-molecule detection [56–60].

3 Objective Lenses and Image Resolution

As mentioned in Sect. 2.3, the objective lens is a key component of any optical microscope and its performance determines the quality of the magnified image.

3.1 Resolution of a Fluorescence Microscope

The purpose of a microscope is to observe small details of the imaged objects. The resolution or resolving power of a microscope, that is the dimension of the smallest detail of the object that can be resolved in the image, is therefore a key indicator of the microscope performance. The higher the resolution, the smaller are the resolvable details, the better. Let us define for simplicity the resolution as the smallest distance between two parallel straight lines that can be resolved as separate lines. This is straightforward enough in theory, less so in an experiment at very high resolutions, where no resolution targets with parallel straight lines of well-defined spacing are readily available. Various approaches how to experimentally measure the resolution in such cases have been developed [61–70], but we will not enter into this topic here.

To characterise the resolution of a fluorescence microscope or in general any optical microscope, we will introduce the concept of the microscope's point spread function (PSF) defined as the image of a point-like object. A hypothetical perfect optical system images each point-like object as a single point, resulting in what we can call a geometrically perfect image. This is however not the case of real optical systems for reasons which we will discuss further.

This concept is particularly relevant in fluorescence microscopy, where each individual fluorophore in the specimen is an independent light source of negligible dimensions. A fluorophore can be approximated as a self-luminous point the image of which is the PSF. The image captured by the microscope is then the sum of images of all fluorophores within the field of view, that means a weighted (by brightness of individual fluorophores) sum of PSFs centred each at the geometrically perfect image of the respective fluorophore. This is mathematically described as a convolution of the geometrically perfect image with the PSF.

Such convolution results in blurring of the image; the broader the PSF, the more blurred becomes the image. Let us consider the hypothetical parallel straight lines; the image of each individual line will not be an infinitely thin geometrical line; it will have the width of the PSF (see Fig. 2). If we start from an infinitely thin line and keep broadening the PSF or decreasing the distance between the lines, the images of the lines will be increasingly overlapped as the PSF width increases with respect to the distance between the lines, until at some point it will not be possible to tell whether there are two closely spaced lines or just a single line.

The next question is what a microscope PSF looks like and by what factors is it determined. To answer it, we need to consider the nature of light as electromagnetic waves. When they propagate through apertures, waves exhibit phenomena referred to as diffraction. Since a microscope objective lens has a finite diameter, it represents an aperture in the optical system and the PSF can be described using the theory of diffraction on a circular (typical cross-section of objective lenses) aperture. The theory predicts that the PSF has the form of an Airy function, which consists of a main central peak and decaying concentric rings. Most of the photons contributing to the image are concentrated in the central peak of the Airy function, making it

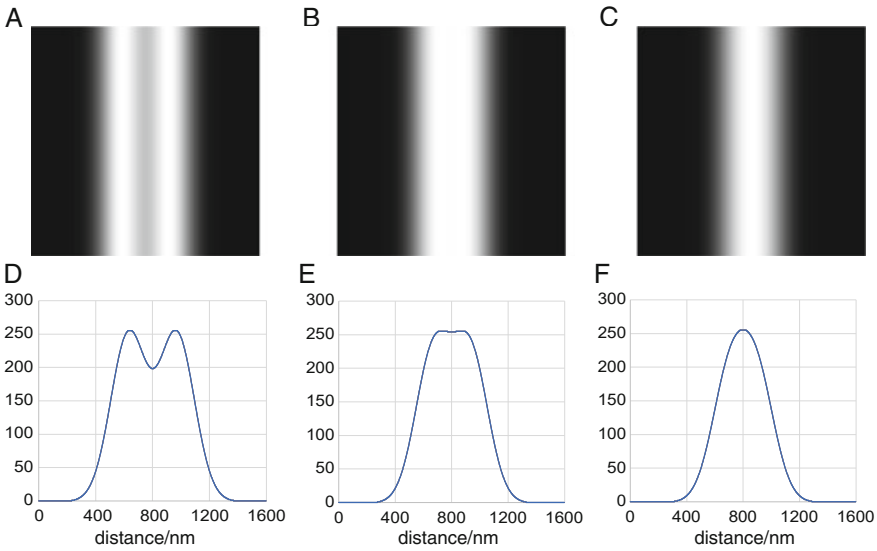

Fig. 2 Diffraction-limited resolution limit illustrated on simulated images of two thin parallel fluorescent lines (**a**–**c**) and the respective intensity profiles along the direction perpendicular to the fluorescent lines (**d**–**f**). The PSF width is $R_{PSF} = 339$ nm. The first case (**a** and **d**) corresponds to the Rayleigh criterion with distance between lines $d = 339$ nm, the second case (**b** and **e**) to Sparrow criterion ($d = 264$ nm) and the last case (**c** and **f**) to unresolved lines at $d = 200$ nm. The dimensions of the images are 1,600 × 1,600 nm. The PSF was for simplicity approximated by a Gaussian function. Intensities in the plots of intensity profiles are shown in relative units

possible to approximate the microscope PSF by a Gaussian function. The smaller the aperture is, the stronger is its effect on the propagation of the waves and the broader is the central peak of the PSF. From what we said earlier, this also means the lower is the resolution.

From the theory of diffraction of light on a circular aperture, it follows that the radius of the PSF central peak R_{PSF}, that is the radial distance between the maximum of the peak and the first minimum of the Airy function is:

$$R_{PSF} = 0.62 \frac{\lambda}{NA}$$

Where λ is the wavelength of the detected light, the florescence wavelength in this case, and NA is the numerical aperture of the objective lens. Because of its influence on the microscope resolution, NA is a key parameter of microscope objective lens performance, and we will discuss it more in Sect. 3.2.

Considering the effect the PSF has on the image of the hypothetical parallel straight lines (see Fig. 2), we can deduce that the microscope resolution d, that is the smallest distance between two lines, at which they can be resolved as separate lines, is proportional to R_{PSF}:

$$d = q\, R_{PSF}$$

The commonly used Rayleigh resolution criterion uses $q = 1$, which means the lines are considered resolvable if the maximum of one PSF coincides with the first minimum of the other PSF [71, 72]. This may be unnecessarily strict, and we may be able to resolve the two lines as separate even if the centres of the respective PSFs are slightly closer. Ernst Abbe in his seminal work [73] derived a formula for microscope resolution, which corresponds to a slightly smaller q:

$$d = \frac{\lambda}{2\, NA}$$

Another commonly used criterion, Sparrow criterion, considers the line to be resolvable as long as the intensity profile along a direction perpendicular to the two fluorescent lines contains two separate maxima with a minimum in between, leading to q of approximately 0.78 (see Fig. 2b, e). In other words, there has to be a dip, no matter how small, in the intensity profile, in order to resolve the lines as separate [71, 72]. This can be considered as an ultimate limit to the resolution. Once the PSFs overlap to such an extent that the intensity profile contains just a single maximum, there is in principle no way how to tell that the image originates from two separate lines and not just from a single, possibly thicker, line (see Fig. 2c, f).

Considering the dip in the intensity profile brings us also to the influence of signal-to-noise ratio on the image resolution. As the distance between the fluorescent lines decreases, so does the difference between the maxima of the intensity profile and the local minimum in between them. When this difference, the depth of the dip, is smaller than the noise in the image, it may not be possible to resolve the dip in the intensity profile and hence to resolve the two fluorescent lines. Sparrow criterion may be therefore perceived as a limit which applies when the signal-to-noise ratio of the image approaches infinity.

Our discussion here dealt only with resolution of two lines which are both in the focal plane, or in other words with the lateral resolution of the microscope. Similar considerations apply also to the resolution along the optical axis. The axial resolution of a microscope objective lens is also determined by its *NA*. For practical purposes, we can consider the diffraction-limited resolution of a high *NA* objective to be approximately 0.2 μm in the lateral and approximately 0.6 μm in the axial direction [71].

3.2 Resolution and Optical Aberrations

The diffraction-limited resolution introduced in the preceding section can be achieved only with an objective lens well corrected for optical aberrations such as astigmatism, field curvature and spherical and chromatic aberrations. From a microscope user's perspective, the last two aberrations are the most important to be aware of.

Chromatic aberration stems from the dependence of refractive index on wavelength of light, known as the chromatic dispersion of a material. Chromatic

dispersion of optical glass results in wavelength dependence of the magnification (lateral chromatic aberration) and focal length (axial chromatic aberration) of a lens. Designers of microscope objectives combine lenses made of glass with different chromatic dispersion to produce a lens assembly with minimal chromatic aberration. Increasing the number of lenses in the assembly allows them to match the magnification and focal length for more individual wavelengths and maintain sufficiently small chromatic aberration for any wavelength in between. Based on the number of wavelengths for which the aberration is corrected, microscope objective lenses are grouped into three categories: Achromats (2 wavelengths), Semi-apochromats or Fluars (3 wavelengths) and Apochromats (≥ 3 wavelengths with stricter limits on the residual aberration) [72, 74]. Besides the number of individual wavelengths for which the chromatic aberration is cancelled out, the different classes of objectives also differ in the spectral range over which the chromatic aberration correction extends. Objectives with a higher class of chromatic aberration correction may be needed when imaging multiple fluorescence channels spanning the whole visible spectrum or even exceeding the visible range, for example to near infrared.

Typically, the residual axial chromatic aberration (see Fig. 3) of corrected objective lenses is more pronounced than the lateral one. In widefield microscopes, the residual axial chromatic aberration can be easily compensated for by adjusting the objective to specimen distance for each channel. This is very straightforward with a motorised microscope, where this task can be automated and does not require the operator's intervention when switching fluorescence channels. It is of course essential to determine correctly the necessary focus shifts, for example by taking images of fluorescent beads labelled by multiple fluorophores which cover all the channels of interest (ideally in the same medium and sample carrier which are used in the actual experiments). This simple solution is, however, not always applicable to confocal microscopy, as we will mention in Sect. 4.4, making apochromatic objectives a preferred choice for confocal imaging.

Spherical aberration is inherent to all optical elements with spherical surfaces, which is the case of nearly all lenses. It is manifested by PSF broadening and therefore, by image blurring and loss of contrast. The general correction strategy relies on combining lenses with positive and negative spherical aberration to produce an assembly with minimal overall aberration. The aberration is wavelength dependent and similarly to chromatic aberration correction, in an apochromatic lens, the aberration is corrected for more individual wavelengths than in an achromatic lens [72, 74]. Beside the optical path within the objective lens, spherical aberration in the image is also affected by the optical path outside of the lens, particularly the part between the fluorophore and the objective lens. Here in general, the light propagates through the specimen, through a coverglass and through an immersion medium, which fills the space between the coverglass and the objective front lens. Of course, in some case there may be no coverglass in between the specimen and the objective lens, which case can be generalised as containing coverglass of zero thickness, or the "covereglass" may not be made of glass but, for example, of polystyrene. Objective lenses are designed to work with (generalised) coverglass of a particular thickness and refractive index and with immersion medium of a particular refractive index.

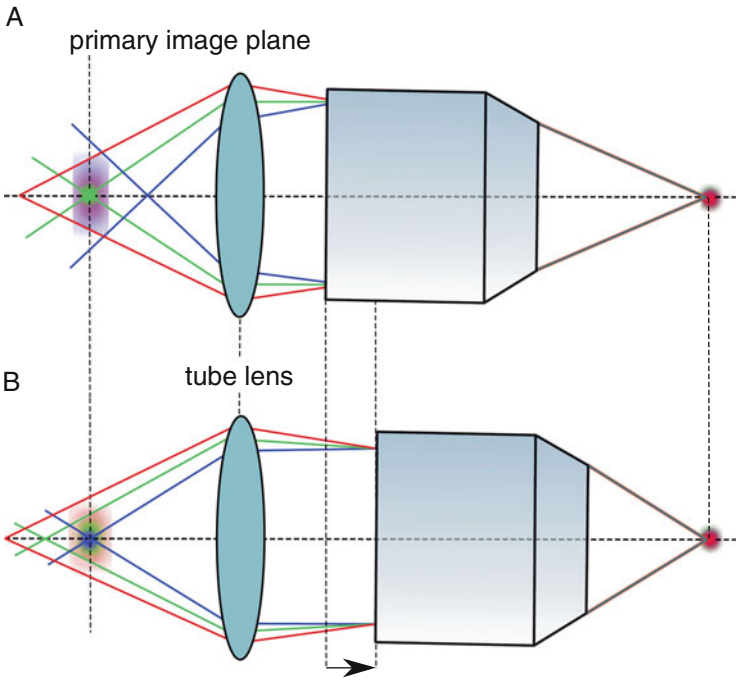

Fig. 3 A schematic illustration of axial chromatic aberration. Fluorophores located in the same plane in the specimen but emitting in different spectral regions are not imaged by the objective lens to the same plane. Thus, if fluorophores emitting in one spectral region, for example the green region (**a**), are sharply focused in the primary image (which also means that the rays of light emitted by them are collimated in the infinity space between the objective lens and the tube lens), fluorophores emitting in the other spectral regions are blurred. By refocusing the objective, fluorophores emitting in another spectral region, for example blue (**b**), can be brought into focus

Spherical aberration correction is compromised if either the coverglass or the immersion medium differ from the expectations. The effect increases with the objective *NA*. Many higher *NA* (> 0.5) lenses are therefore equipped with a correction collar that allows the user to tune the spherical aberration correction to work optimally with coverglass of different thickness and material and/or with different immersion media [72]. There are, for example, objectives which can be used with water, glycerol, or microscopic oil as immersion, as well as air immersion objectives which can accommodate a broad range of coverglass thickness from 0 to 1.2 or 1.5 mm. The quality of images produced by low *NA* objective lenses depends only marginally on the coverglass thickness; therefore, such lenses are usually not equipped with adjustable correction.

Other than the immersion medium and the coverglass, the specimen itself and its optical properties affect the spherical aberration correction [75]. In general, the correction performs the best if there is no refractive index difference between the specimen and the immersion medium. For this reason, specimens for high-resolution microscopy are often mounted in media with carefully tuned refractive index

[76]. The effects of the specimen refractive index increase with the length of the optical path within the specimen, or in other words, with the depth within the specimen at which we focus. When imaging, for example, a specimen in an aqueous medium, at shallow depths (units of μm), an oil immersion objective is likely to slightly outperform a water immersion one because of the former's higher *NA*; however, at larger depths (10s of μm and more) a water immersion objective is likely to largely outperform an oil immersion counterpart because of the increasing spherical aberration in the latter case.

Since the specimen-induced aberrations are specific to the specimen, more precisely to a specific location within the specimen, no generic correction scheme can be incorporated in the design of the objective lens. Adaptive optics offer a possible solution as they allow to tune to correction for each individual location in the specimen and different strategies have been developed for finding a good correction without adding too much to the time needed for image acquisition [77–80].

3.3 Objective Lens Numerical Aperture

NA of an objective lens is defined as the product of the immersion medium refractive index n and $\sin\theta$, where θ is the largest possible half angle of the cone of light that can enter the objective lens:

$$NA = n \sin\vartheta$$

The importance of the refractive index of the medium is illustrated in Fig. 4. It shows how rays of light are bent by refraction on interfaces between media of different refractive indices, as described by Snell's law. In this way, the oil immersion objective working with immersion medium of a higher refractive index effectively collects light emitted by the fluorophore into a larger solid angle. This means that the larger the *NA*, the higher is the objective's light collection efficiency and the brighter is the image formed by such a lens. This is a very important consideration in fluorescence microscopy where the photon budget is limited.

As we noted in Sect. 3.1, *NA* also determines the resolution of the objective lens. This, together with its impact on light collection efficiency, makes *NA* probably the single most important parameter describing objective lens performance. The influence of objective *NA* on microscope resolution follows also from an information-theory point of view. Higher resolution means higher information contents of the image; since photons are the information carriers in optical microscopy, collecting a larger portion of all photons emitted by the fluorophores in the microscope field of view does not increase only the brightness but also the resolution of the image.

From geometrical considerations, it follows that to maximise *NA*, it is necessary to minimise the distance between the fluorophore and the objective front lens, that is the working distance of the objective. This is not always possible because of steric constraints imposed by the specimen. In some situations, where long working

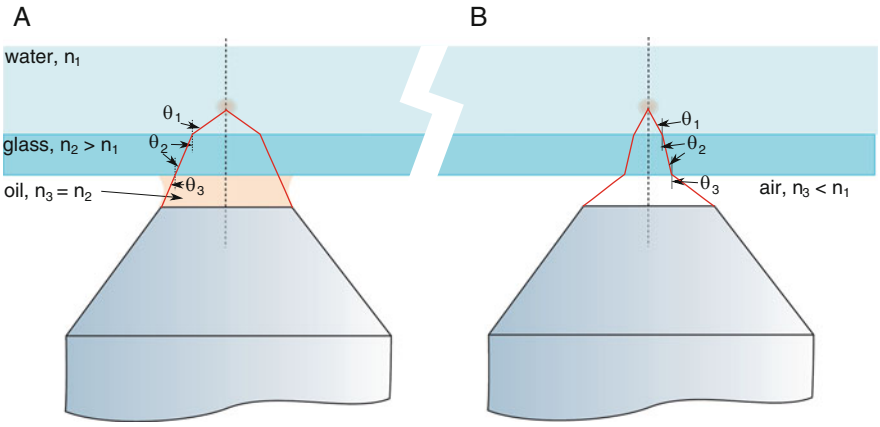

Fig. 4 A schematic illustration of the influence of the refractive index of the immersion medium on the light collection efficiency of an objective lens as expressed by the objective's *NA*. As the rays of light pass across interfaces between different media, the product $n \sin \theta$ remains constant as predicted by Snell's law. As a result, an oil immersion objective (**a**) can collect light emitted by the fluorophore into a larger solid angle than a similar air objective (**b**)

distance of the objective lens is necessary, *NA* has to be compromised and together with it the light collection efficiency and the resolution of the objective.

From the definition of *NA*, it is clear that since $\sin\theta < 1$, $NA < n$. This is true for a single-objective lens. However, by using multiple objective lenses, each with $NA < n$, it is possible to construct a microscope with overall higher *NA*, equal to the sum of the *NA*s of the individual objectives. In this way light emitted by the fluorophores into a larger solid angle can be collected and the resolving power of the microscope enhanced. This approach is referred to as 4Pi-microscopy in allusion to the full solid angle of 4 π, an ultimate goal that is in practice not achievable. High *NA* objective lenses tend to be quite bulky limiting practically the number of objectives that can be thus combined to two in most cases [71, 81, 82].

3.4 Resolution and Image Pixel Size

So far, we have only considered the details resolvable in the image generated by the microscope optics in the primary image plane. There is, however, one more step involved in capturing the image, which can also affect the resolution of the final digital image. In a widefield microscope, the primary image is captured by a camera sensor consisting of discrete physical pixels. Features in the primary image that are detected by a single physical pixel are not resolvable in the digital image. To discuss this topic, we will introduce the projected pixel dimension p_S, which is the physical pixel pitch p_C divided by M, the microscope's total magnification (the product of the magnifications of the objective lens and any additional magnifying or demagnifying

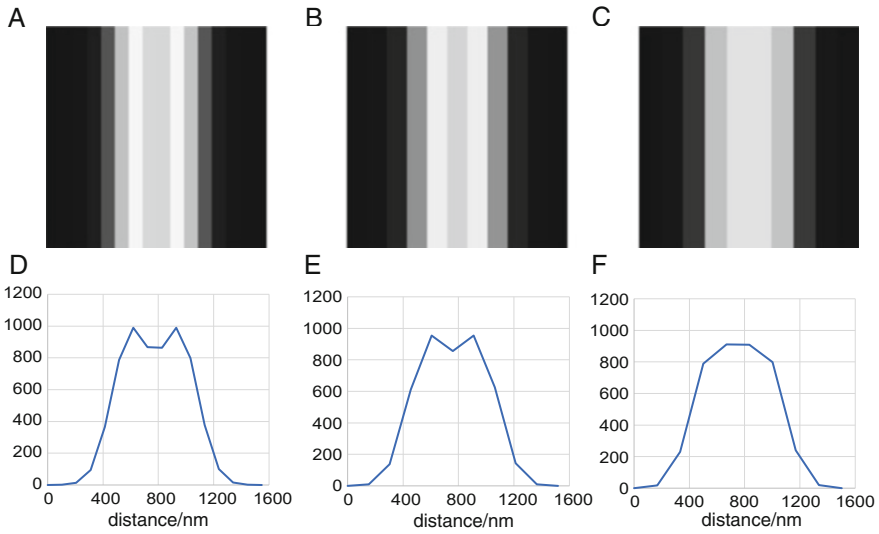

Fig. 5 The influence of the projected pixel size on image resolution illustrated on simulated images of two thin parallel fluorescent lines (**a**–**c**) and the respective intensity profiles along the direction perpendicular to the fluorescent lines (**d**–**f**). The simulated situation is identical to that shown in Fig. 2 **a** and **d** (the PSF width is $R_{PSF} = 339$ nm and the distance between the lines $d = 339$ nm); however, this time the effect of different projected pixel size p_s is simulated. Images and intensity profiles for $p_s = 103$ nm (**a** and **d**), 152 nm (**b** and **e**) and 167 nm (**c** and **f**) illustrate that the two lines can be resolved only if p_s is smaller than half of the distance between the lines. It should be noted also that in the case of pixel-size limited resolution, it is the distance of features in the primary image, rather than the distance of the actual structures in the specimen that matters. The overlap of the PSFs results in the intensity maxima being closer to each other (approximately 318 nm) than the distance of the underlying thin lines. The same effect can also lead to overestimation of resolution if it is measured directly as the shortest distance between resolvable features in an image. The dimensions of the images are 1,600 × 1,600 nm. The PSF was for simplicity approximated by a Gaussian function. Intensities in the plots of intensity profiles are shown in relative units

optics between the objective lens and the camera). It is, therefore, the dimension of the area in the sample, which is captured by a single camera pixel. Let us again consider the case of the two parallel lines, this time separated by a distance larger than the diffraction-limited resolution. As seen in Fig. 5c and f, when p_S is larger than half of the distance between the lines, the lines appear as a single line in the image. This is a demonstration of the Nyquist-Shannon sampling theorem. A diffraction-limited image is therefore obtained only if p_S is smaller than half of the resolution limit d, or in other words:

$$d > \frac{p_C}{2M}$$

4 Confocal Microscopy

One of the weaknesses of widefield epifluorescence microscopy, which we have discussed so far, is its susceptibility to high background originating from out-of-focus planes, especially when imaging thicker specimens. The cause of this problem is illustrated in Fig. 1a. Fluorescence is excited in the whole volume of the specimen that is illuminated by excitation light, which means that fluorophores in planes below and above the focal plane emit as bright fluorescence as fluorophores in the focal plane. Rays of light emanating from a fluorophore in the focal plane are collimated by an infinity corrected objective lens and then focused by a tube lens to the plane of a camera sensor, where they generate, in the ideal case, a diffraction-limited spot, the PSF of the microscope. Fluorophores located at different positions in the focal plane are imaged as PSFs at different positions in the plane of the camera sensor and together all these PSFs add up to a sharp, meaning diffraction limited, image. However, rays coming from fluorophore in out-of-focus planes are not collimated by the objective lens, they are either divergent or convergent in the infinity space. As a result, the signal from such fluorophores is spread over larger areas in the plane of the camera sensor, contributing blurry background to the image.

A commonly used solution to this problem is based on blocking the out-of-focus light by a spatial mask with an aperture positioned in such a way to selectively transmit the signal originating from the focal plane. This is the principle of confocal microscopy as illustrated in Fig. 1b. In this case a mask with a small aperture is placed in the primary image plane instead of a camera sensor. Rays originating from a fluorophore located in a corresponding spot in the focal plane are tightly focused in the plane of the mask and, therefore, pass through the aperture to the detector. On the other hand, light emanating from fluorophores in out-of-focus planes is defocused in the plane of the mask and only a small fraction of it can pass through the aperture.

We can notice that with a single aperture, only light coming from a single position within the focal plane can make it through the aperture. Rays from other locations within the focal plane, though focused in the plane of the mask, would not coincide with the aperture and would, thus, be completely blocked. This means that in such a configuration, we are not able to directly capture an image; instead, we are measuring the fluorescence intensity originating from a single small detection volume in the specimen. While this is clearly useful for various forms of fluorescence micro spectroscopy, such as single-point FCS, it is clearly not a complete solution to the problem of blurry background in widefield images. To get a confocal fluorescence image, we need to scan the specimen with the confocal detection volume and measure the fluorescence intensity for each position, that is for each pixel (or each voxel in the case of 3-dimensional imaging). Before we proceed to scanning the specimen, let us make a few additional observations:

1. Since fluorescence is collected only from a small effective detection volume, it would be wasteful to excite the whole volume of the specimen and subject it unnecessarily to photobleaching of fluorophores and photo-toxic effects. Instead, fluorescence is excited by a focused (typically laser) beam. The highest excitation

efficiency is achieved in the focus of the beam which is aligned to correspond to the effective detection volume defined by the aperture; the excitation beam focus and the aperture are therefore said to be confocal with respect to each other. The focused excitation further confines the effective excitation volume.

2. Since we are capturing the intensity from a single-detection volume at a time, there is no need for a spatially resolved light sensor. A single-point detector of light is enough in this case. Photomultiplier tubes (PMTs) are commonly used in point-scanning confocal microscopy (and other point-scanning microscopy modalities, see Sect. 5.1). PMTs with GaAsP cathodes have become very common, replacing, the previously most widespread, multi-alkali PMTs. GaAsP PMTs offer higher QE compared to multi-alkali PMTs (over 40% across most of the visible spectrum). Even higher QE is offered by single-photon avalanche photodiodes (SPADs), which however suffer from lower dynamic range and have been preferred predominantly for low-light photon counting applications [83]. Hybrid detectors combining technologies (and to a large extent also the advantages) of SPADs and PMTs are replacing SPADs in many microscopy applications. Another perspective technology of point-detectors are silicon photomultipliers (large arrays of SPADs), attractive for their larger active areas, higher dynamic range and low cost [84–86].
3. The size of the confocal aperture affects the efficiency of rejection of out-of-focus light as well as the light collection efficiency. As said earlier, the image of an in-focus fluorophore is the microscope PSF. Most of the light forming the image is concentrated in the PSF central peak. Setting the aperture size such that it admits the whole central peak of the PSF but not more, therefore, ensures that nearly all signal from the in-focus fluorophores is collected without admitting more out-of-focus light than necessary. Such aperture size is referred to as 1 Airy unit (1 AU), a relative unit deriving its name from the Airy function describing the PSF. Increasing the aperture size above 1 AU increases only marginally the collection efficiency of light from in-focus fluorophores, while having a larger impact on the out-of-focus light collection efficiency. In this way the rejection of out-of-focus light and the optical sectioning capability (see Sect. 4.5) of the confocal microscope are compromised with little gain in in-focus signal. On the other hand, apertures smaller than 1 AU effectively reduce the detection volume, thus, improving the resolution of the image in both the lateral and the axial direction [87–89]. This resolution improvement, however, comes at the cost of reduced signal since, even for a fluorophore located ideally in the objective lens focus, only a portion of the signal contained in the PSF central peak can be detected. Since the photon budget in biological fluorescence microscopy is usually quite limited, apertures of approximately 1 AU are usually chosen as a good compromise between requirements on resolution and sectioning on one side and on signal on the other side.
4. A detector with a small active area or an optical fibre can also act as a confocal aperture [90]. The disadvantage of the former solution is its limitation to a single detector. When using a mask with an aperture or an optical fibre, the signal can be spectrally divided by secondary dichroic mirrors or by a dispersive element (a prism or a grating) onto multiple detectors for simultaneous detection of distinct fluorophore species.

5. The pixel-wise manner of image acquisition makes point-scanning microscopy modalities the usual choice for implementing any type of micro spectroscopy imaging. Any type of spectroscopy can be readily applied on the signal that passes through the confocal aperture, which may not be easily doable when the whole image is captured at once by a camera. For these reasons, for example FLIM (see chapter "Time-Resolved and Polarized Spectroscopy") is typically performed in a point-scanning manner, although cameras capable of time-resolved fluorescence detection exist and have become commercially available and are likely to become more widespread [91, 92].

One possible approach to confocal scanning uses mechanical movement of the specimen with respect to the microscope objective, usually using a piezo positioner. Either the sample stage or the objective lens can be the moving part. Because of its slower speed, this form of scanning is rarely used in biological confocal microscopy. It is convenient, for example in correlative confocal fluorescence and atomic force microscopy (AFM), because the physical movement of the specimen with respect to the cantilever is required in AFM [93].

4.1 Laser Scanning Microscopy

Faster scanning is achieved by moving the excitation beam and leaving the objective lens and the specimen stationary. Microscopes employing this form of scanning are called laser scanning microscopes and are routinely used in biological imaging [94]. The scanning is realised by deflecting the laser beam to different points in the focal plane with a pair of mirrors rapidly moved by a galvanometer drive. When driven at their resonant frequencies, such mirrors can scan several thousand lines per second. Fluorescence emitted from the laser focus then follows the reverse path of the excitation laser beam and is deflected by the scanning mirrors (so-called de-scanned) to the confocal aperture. The confocality of the laser focus and the aperture is, therefore, maintained for an arbitrary position within the scanned area.

As with any other point-scanning microscopy technique, the speed of scanning determines the time needed to scan an image as well as the pixel exposure time. While fast scanning with resonant scanners gives short image acquisition time (or in other words high frame rates) which compare favourably with non-scanning imaging modalities, the pixel exposure times are necessarily extremely short and, considering typical fluorescence photon fluxes, repeated scanning with averaging is typically needed to collect sufficient signal. At a first glance such fast scanning rates may not, therefore, look particularly useful if they require repeated scanning, which reduces the effective frame rate. Yet, it has been shown that there are advantages to very fast, even if repeated, scanning. Most fluorophores exhibit some form of dark or dim states, to which they enter through the excited state. Under continuous excitation, there exists an equilibrium between the fluorophore populations in the bright and the dark states. Fluorophores in the dark state do not contribute to the fluorescence signal and their fraction, thus, reduces the effective fluorophore brightness. Since they enter

the dark state through the excited state, in the absence of excitation, there is no dark state population (all fluorophores are in the ground state ready for excitation). This means that in a short time after the excitation has been turned on and before the equilibrium dark state population has been established, the effective fluorophore brightness is transiently higher. Going back to confocal scanning, the higher the scanning speed, the more is this transient phase represented in the pixel exposure time, giving typically a higher effective fluorophore brightness [95].

4.2 Image Sampling and Magnification in Point-Scanning Microscopy Modalities

In Sect. 3.4 we have discussed the influence of the projected pixel size p_S on the resolution of the captured digital image and concluded that in order not to compromise the optically achievable resolution d, p_S needs to be equal to or smaller than half of d. This is a general conclusion which holds for point-scanning microscopy modalities as well. However, unlike in widefield microscopy, where p_S is determined by the interplay between the microscope magnification and camera pixel pitch (and microscope operator thus can do little about it), in point-scanning microscopy modalities the microscope operator has a full control over p_S, which is flexibly determined by the scanning settings. This gives the microscope operator the power to intentionally (or unintentionally) over- or under-sample the image. Undersampling, using too large p_S, compromises the image resolution; oversampling, on the other hand, increases unnecessarily image acquisition time by scanning more lines and typically also compromises signal-to-noise ratio by reducing pixel integration time (unless scanning speed is reduced correspondingly, further increasing the acquisition time) and the effective area from which the signal in each pixel is collected. The optimal p_S is therefore only slightly smaller than $d/2$.

Another observation, worth making at this point, is the relative unimportance of objective lens magnification in point-scanning microscopy modalities. The actual magnification of the acquired image is defined by the sweep of the scanner, which can be nearly arbitrarily reduced to increase magnification. The objective lens magnification determines only the maximum dimensions of the scanned area, that is the minimum magnification possible. Since resolution and light collection efficiency is determined solely by the objective's *NA*, lower magnification objectives with high *NA* are the most flexible solution for point-scanning microscopy modalities and advantageous over higher magnification objectives of the same *NA*.

4.3 Spinning Disk Confocal Microscopy

The speed of point-scanning confocal microscopy is necessarily limited by the pixel-wise image acquisition, which, especially for larger fields of view, can significantly limit the achievable temporal resolution. An obvious way to overcome this limitation

and increase the acquisition speed lies in multiplexing the confocal image acquisition, that means in acquiring signal at multiple points simultaneously. A variety of multiplexed confocal designs have been proposed including line-scanning confocals [96–100], which illuminate a whole line in the focal plane and replace the confocal aperture with a confocal slit; however, the most widespread design is a spinning disk confocal microscope [101, 102]. The design has quite a long history starting in the 1960s [103, 104], although it was only much later that is became widespread.

A typical spinning disk confocal microscope uses a disk with pinholes arranged in a spiral pattern rotating at a high speed. The disk has the dual purpose of defining the positions of excitation foci and rejecting out-of-focus fluorescence. As the disk rotates, the excitation foci move over the focal plane, until every point within the field of view has been exposed to excitation. The in-focus fluorescence, which passes through the disk, is focused on a camera sensor. As the camera is exposed throughout the rotation of the disk, a complete image of fluorescence from the focal plane builds up within the camera exposure time. Some designs feature a second disk with micro lenses, which focuses the excitation laser beam on the pinholes in the main disk. This ensures that the excitation light is not wasted and alleviates the requirements on laser power.

4.4 Chromatic Aberration in Confocal Microscopy

As we mentioned in Sect. 3.2, simple refocusing may not be a sufficient solution to compensate for residual axial chromatic aberration of the objective lens in confocal microscopy. Let us get back to that point and explain why it is so and at what situation it is particularly problematic. In a widefield microscope, fluorescence is excited uniformly in the entire depth of the specimen (provided the specimen is sufficiently transparent). Therefore, chromatic axial aberration is relevant only for fluorescence emission to make sure fluorescence in all channels is collected from approximately the same focal plane within the specimen. In a confocal microscope, on the other hand, the excitation beam is focused into the focal plane, making excitation most efficient in that plane. It is therefore desirable that axial chromatic aberration is corrected also for the excitation wavelength to ensure confocality of the excitation laser beam and the aperture for all channels.

This may can be problematic when working, for example with fluorophores excited in the UV part of the spectrum, such as many popular DNA labelling dyes emitting in the blue to green range of the visible spectrum. At confocal microscopes, such dyes are usually excited with a 405 nm laser line, which lies outside of the corrected range of Achromats, Semi-apochromats, and even older Apochromats. The axial chromatic aberration can increase quite steeply towards shorter wavelength outside of the corrected range resulting in axial distances of several μm between the foci of the 405 nm laser line and of those laser lines which lie within the corrected range (see Fig. 6a for a schematic illustration).

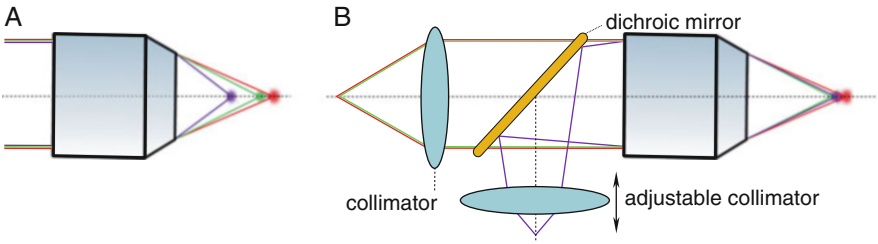

Fig. 6 A schematic illustration of axial chromatic aberration in confocal microscopy (**a**) and an approach to reducing it by using separate collimators for different laser lines. Axial chromatic aberration causes the foci of different laser lines to lie at different axial positions (**a**). This effect can be very significant for laser lines outside of the corrected spectral range of the objective lens. 405 nm laser line (represented in purple in the figure) is outside of the corrected range of many objective lenses; therefore, in many confocal setups, it is delivered to the objective following a separate optical path with a separate collimator (**b**). The beam entering the objective can be, thus, made divergent or convergent, resulting is moving the focus along the optical axis (the more divergent the beam is, the further is the focus from the objective lens and vice versa). By tuning the collimator for the 405 nm laser line, its focus can be overlapped with the foci of the remaining laser lines. A dichroic mirror is used to merge the optical path of the 405 nm laser line with the path of the other laser lines. Note that the depicted dichroic mirror is not the main dichroic mirror, which separates the excitation and emission paths and which was omitted for simplicity in the figure. The main dichroic mirror would be located between the depicted excitation dichroic and the objective lens

Alternatively, if the 405 nm line follows a different optical path with a different collimator than the rest of the laser lines, its focus can be tuned to overlap with the focus of the other laser lines by adjusting the dedicated collimator (see Fig. 6b). This solution has been adopted by many commercially available laser scanning microscopes.

4.5 Optical Sectioning and Volumetric Confocal Imaging

By rejecting out-of-focus fluorescence, a confocal image effectively contains the signal only from a thin section of the specimen (approximately 0.5 μm with high *NA* objective lenses) [105]. This property of confocal microscope is usually referred to as optical sectioning in contrast to actual physical sectioning (cutting the specimen into thin slices) often used to produce background-free images of thick specimens. By focusing the microscope into different planes within the specimen, the whole volume of the specimen can be imaged and a 3-dimensional image rendered from the optical sections. Focusing the microscope into different planes is usually realised by moving either the objective or the specimen stage along the optical axis. Alternatively, tuneable or variable-focus lenses can be employed to modify the focal length of the imaging optical system [106, 107]. This approach eliminates mechanical moving parts and allows for very fast switching between different focal planes.

However, by tuning the focal length of the imaging optics, the magnification, NA and aberration corrections are also affected, restricting the usable range of this approach.

Acquiring a 3-dimensional image of a relatively large specimen can be a time-consuming task as it requires capturing many optical sections, each of which may take a non-negligible time to capture, especially in the case of point-scanning confocal microscopes. Beside the time needed, photobleaching is another concern. Although the excitation in a confocal microscope is the most efficient in the focal plane, the excitation efficiency does not drop sharply away from that plane and fluorophores are excited, hence potentially bleached, across the thickness of several optical sections above and below the focal plane. Fluorophores in the sections imaged later in the course of the acquisition may be thus considerably bleached out by imaging of the preceding sections. In response to these concerns, several designs of multifocal confocal microscopes have been proposed, neither having yet become widely used [108–110]. Another technique addressing, among other, these concerns is lightsheet microscopy, also known as selective plane illumination microscopy (SPIM). SPIM has become a well-established alternative to confocal microscopy for 3-dimensional imaging and we will return to it in Sect. 5.2.

Another issue faced not only by confocal microscopy when performing 3-dimensional imaging, is the limited penetration of light into specimens that are not transparent. As the optical path through the specimen increases, larger fractions of both the excitation light and the fluorescence are scattered and/or absorbed by the specimen leading to decaying signal-to-noise ratio of the image. This is especially prominent in the case of optically dense samples such as tissue. A confocal aperture can help to some extent by screening out scattered photons, which would otherwise increase the background. However, when photons emitted by an in-focus fluorophore are scattered, their paths are altered and they are likely not to reach the confocal aperture and not to contribute to the detected signal. In this way, the signal is gradually lost in confocal microscopy with increasing depth in the specimen.

One way to overcome this limitation is based on making the specimen optically transparent by tissue clearing [111]. This approach is however not compatible with live samples. Other approaches utilise the fact that light scattering efficiency decreases with increasing wavelength. Infrared light thus penetrates considerably deeper into tissue or other non-transparent specimens than visible light. Near-infrared confocal microscopy is therefore better suited for imaging such specimens than confocal microscopy in the visible range [112–115]. The longer the excitation and emission wavelengths are, the deeper is the penetration depth. Practical limitations stem from the restricted choice of suitable fluorophores rather than from the microscopy hardware side. A popular alternative is multi-photon fluorescence microscopy which allows excitation of standard visible fluorophores by infrared light as we describe in Sect. 5.

Adaptive optics can also help to compensate for the effects of light scattering by the specimen [77–79, 116].

5 Other Modalities with Optical Sectioning Capabilities

5.1 Multi-Photon Fluorescence Microscopy

A fluorophore can be excited by simultaneously absorbing multiple (n) photons. Assuming all the n photons having the same wavelength and therefore the same energy (which is in general not necessary), each photon contributes $1/n$ of the excitation energy. Since photon energy is inversely proportional to the wavelength, the wavelength of each of the n photons can be n times longer than the wavelength of a single photon that would be needed to excite the molecule by single-photon absorption. Therefore, Stokes shift is reversed in the case of multi-photon fluorescence excitation and the fluorescence has shorter wavelength than the excitation. Visible fluorescence can be thus excited by infrared light. Since simultaneous absorption of n photons is needed, multi-photon excitation requires much higher excitation light intensities than single-photon excitation. The excitation efficiency in multi-photon fluorescence scales with the n^{th} power of the excitation intensity, making it an example of non-linear optical phenomena (that means optical phenomena where the response magnitude, such as the fluorescence intensity, depends on the excitation intensity in a non-linear way). Obviously, the excitation intensity needed grows with the the photon number n. Practical considerations regarding the necessary excitation light sources limit the photon numbers n used in multi-photon fluorescence microscopy to 3 at most, with 2-photon microscopy being by far the most common case of multi-photon microscopy [117, 118].

To achieve excitation intensities high enough for multi-photon excitation to occur, the excitation photon flux is typically concentrated both in time and space. The former is realised by using pulsed lasers with very short pulses (approximately 100 fs) and high peak power. Besides tuneable Ti-sapphire lasers, which are the most common example of such excitation sources for multi-photon microscopy, single-wavelength fibre lasers have emerged as a cost-efficient alternative [119]. The latter is achieved by tightly focusing the excitation laser beam to a diffraction-limited spot, similarly to laser scanning confocal microscopy. Images are then acquired by point-by-point scanning as discussed in Sect. 4.1. Although most multi-photon microscopes rely on point-by-point scanning, 2-photon microscopy has been implemented also in widefield [120–125] or line-scanning [126, 127] configurations.

As mentioned in Sect. 4.5, multi-photon microscopy is commonly used for 3-dimensional imaging of highly scattering specimens, because of the increased penetration depth of infrared light. This may not seem at first a sufficient solution of the scattering issue since the fluorescence in multi-photon microscopy is in the visible range, hence equally susceptible to scattering as fluorescence in single-photon confocal microscopy. To fully understand the benefits of multi-photon microscopy, we need to realise that because of the non-linear nature of the excitation process, excitation efficiency decays sharply with increasing distance from the focal plane. This effectively ensures optical sectioning without the need for a confocal aperture. Removing the confocal aperture enables the collection of a larger fraction

of photons emitted by in-focus fluorophores. To maximise the fraction of collected scattered fluorescence photons, the detectors in multi-photon microscopy are often placed as close as possible to the objective lens. Since the collected fluorescence light does not need to reach the confocal aperture, it does not have to pass through the scanner to be de-scanned as in laser scanning confocal microscopy. Instead, all the fluorescence collected by the objective lens is focused onto the detector active area. This configuration known as non-descanned detection is common in multi-photon microscopy [128, 129].

Another application that benefits from multi-photon microscopy is imaging of UV-excitable fluorophores, which cannot be efficiently excited at a confocal microscope. This is the case of many intrinsic fluorophores, making multi-photon microscopy a good solution for label-free fluorescence studies of cells and tissues [130–133].

5.2 Lightsheet Microscopy

Unlike the other fluorescence microscopy modalities introduced in this chapter, lightsheet microscopy or selective-plane illumination microscopy (SPIM) does not use episcopic geometry. Instead, the excitation and the emission light paths are oriented perpendicularly to each other as show schematically in Fig. 7. The concept appeared for the first time in 1903 [134], after which it has been practically forgotten until further developments about a century later [135, 136]. Since then, lightsheet microscopy has become a well-established technique for rapid 3-diemnsional fluorescence imaging, which had a large impact in many biological fields, in particular in developmental biology.The broad range of specimens and topics studied by lightsheet microscopy led to the developments of various microscope designs suited optimally for certain ranges of applications. Reviewing all the modalities of lightsheet microscopy is beyond the scope of this section; more can be found, for example in recent reviews [137, 138]. In essence, in a lightsheet microscope, the light from an excitation source (a laser in the modern implementations) is focused by illumination optics to generate a thin sheet of light (hence the name of the technique) which excites fluorescence in a layer of the specimen (an optical section) and the fluorescence is imaged by an objective lens placed perpendicular to the lightsheet and detected by a camera. In its simplest form, the illumination optics consist of a single cylindrical lens which focuses a collimated beam of light into a sheet of light (as opposed to the more common spherical lenses which focus a collimated beam into a single spot). Other optical elements can be added to produce thinner lightsheets or increase the extent of its usable area [139, 140]. By the usable area, we understand here the portion of the lightsheet around its focus where the thickness of the lightsheet can be considered reasonably uniform (see Fig. 7). Illumination is often provided from two or more opposing sides of the specimen to avoid shades resulting from limited penetration of the lightsheet into larger specimens [141, 142]. Various designs of single-objective lightsheet microscopes in which a

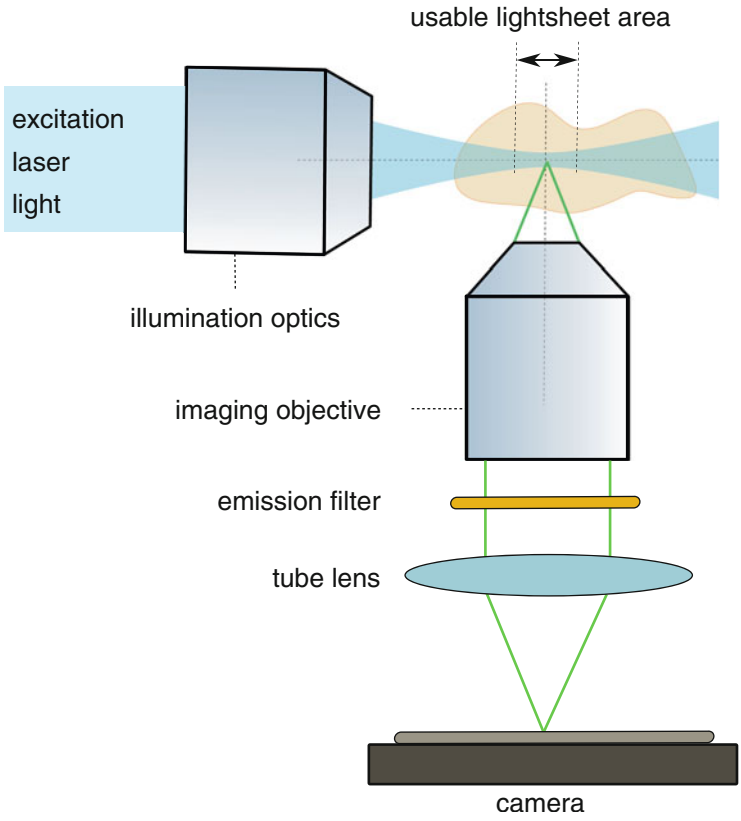

Fig. 7 A schematic illustration of a generic lightsheet microscope. The illumination optics produce a sheet of excitation light which excites fluorescence in a section of the specimen. The fluorescence is imaged by an objective lens placed perpendicularly to the lightsheet. See Sect. 5.2 for more details

single-objective lens provides excitation and detection similarly to a standard epifluorescence microscope, are a notable exception to this generic scheme [143–146]. Different variants of lightsheet microscopes differ in various aspects of their designs such as:

1. Orientation of the lightsheet (vertical, horizontal, or slanted) chosen according to the way the respective specimens are typically mounted.
2. Thickness and the extent of the usable area of the lightsheet. In general, the higher is the *NA* of the illumination optics that create it, the thinner is the lightsheet and at the same time the smaller is its usable area. For large specimens such as whole cleared organs, thicker lightsheets (several µm) with larger usable area are preferable; such setups are often referred to for historical reasons as ultramicroscopes [147]. Imaging of small specimens such as live cells, benefits from thinner, sub-µm optical sections [148]. To increase the illumination *NA*, thus

reducing the lightsheet thickness, objective lenses are usually added to the illumination path as the last optical element before the specimen. Thin lightsheets with increased usable areas can be produced from beams other than Gaussian beams, which are the most common beams produced by lasers. Notable examples are Bessel beam lightsheets [149] and lattice lightsheets produced by interference of multiple Bessel beams [148]. Such lightsheets improve the sectioning capability without compromising the field of view.

3. The mode in which the lightsheet is generated. The original lightsheet microscopes used a static lightsheet which illuminates simultaneously the whole optical section. Later an alternative scheme has been introduced in which the lightsheet is created by rapidly scanning a beam along a line [126, 149, 150]. This approach prevents striping artefacts which can occur when different parts of a static lightsheet interfere with each other after being perturbed by the specimen.

3-dimensional imaging with a lightsheet microscope is usually realised by mechanically moving either the specimen or the lightsheet with respect to the other. Different optical sections are therefore acquired sequentially like in a confocal microscope; however, non-illuminated sections are not subject to bleaching. Methods to increase the throughput of lightsheet imaging by parallel multi-plane imaging have been proposed [151–153].

5.3 Total Internal Reflection Fluorescence Microscopy

This technique uses the phenomenon of total internal reflection which can occurs at the interface of two media with different refractive indices. When light propagating from the medium of higher refractive index hits such an interface under a sufficiently large angle, the angle of refraction predicted by Snell's law is larger than a right angle and, in that case, there is no refracted beam propagating into the medium of lower refractive index. The beams are only reflected into the medium of higher refractive index, hence total internal reflection. However, wave optics predict that some energy of the impingent wave enters the medium of lower refractive index in the form of an exponentially decaying wave, called the evanescent wave (see Fig. 8a). The penetration depth can be tuned by the angle of incidence to be a fraction of the incident light wavelength. Since evanescent wave can excite fluorophores present only within a very thin layer of the lower refractive index medium close to the interface, total internal reflection fluorescence (TIRF) can be used for selective imaging of such fluorophores.

In practice, the higher refractive index medium is usually a microscope coverslip and the lower refractive index medium is an aqueous medium of the specimen. High *NA* oil immersion objectives are used to support illumination under sufficiently large angles. TIRF clearly outperforms confocal microscopy or lightsheet microscopy in terms of thinness of the optical section; however, the said section is limited to the vicinity of the coverslip surface. This makes TIRF the technique of choice for single-

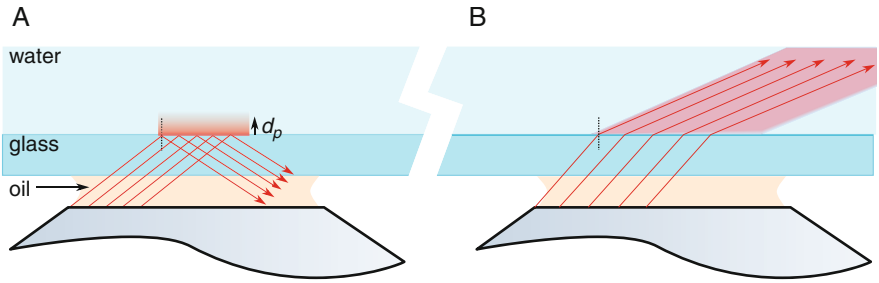

Fig. 8 A schematic illustration of TIRF (**a**) and HILO (**b**) microscopy. See the text of Sect. 5.3 for more details. d_p denotes the penetration depth of the evanescent field (**a**)

molecule imaging and cell membrane studies [44, 154–159]. When the incidence angle of the excitation beam is slightly larger than the critical angle needed for total internal reflection, refracted beams propagate into the specimen under a very large angle, that means in a direction nearly parallel to the interface. In this way, fluorescence can be excited in a section reaching deeper than the evanescent field penetration (see Fig. 8b). This approach is referred to as highly inclined and laminated optical sheet (HILO) and is useful when the structures of interest lie slightly further from the coverslip surface [160, 161]. A related approach called super-critical angle fluorescence (SAF) uses the fact that a part of the light emitted by fluorophores very close to optical interfaces propagates at directions nearly parallel with the interface. By collecting only light propagating under such angles, fluorophores located in a thin layer close to the interface are selectively imaged [162–165].

5.4 Structured Illumination

Structured illumination represents a widefield solution facilitating the discrimination of in-focus fluorescence from the out-of-focus background. It uses spatially modulated excitation illumination, with the spatially modulated pattern being focused in the objective focal plane. Hence the in-focus fluorescence is also spatially modulated and the modulation decreases with the distance from the focal plane. Since the fluorescence image is spatially modulated, multiple images with different positions of the modulated pattern need to be acquired to reconstruct a non-modulated image of the in-focus fluorescence. The sparser is the illumination pattern, the more efficient is the background removal, but at the same time, a higher number of modulated images is needed to reconstruct a non-modulated image. In the case of a pattern consisting of alternating bright and dark stripes of equal width, the minimal number of modulated images needed is three [166]. A related approach called aperture correlation microscopy uses a similar image reconstruction strategy and a spinning disk with slit apertures to produce the modulated excitation [167].

Note that structured illumination is also used to increase the resolution of microscopy images, as we will discuss in Sect. 6.3. In that case the requirements on excitation pattern spatial modulation frequency and the number of images acquired are in general higher than if only optical section is aimed at.

5.5 *Computational Approaches*

The easiest, though of course not necessarily the most powerful, way to remove out-of-focus background from a widefield fluorescence image is by simply subtracting an estimate of the background from the image [168, 169]. A common way to do this known as unsharpen mask estimates the background as a blurred version of the image itself. The image can be blurred, for example by replacing each pixel value with the median or a (weighted) average of pixels in its neighbourhood; the larger the neighbourhood considered, the more smoothed-out is the resulting image. The blurred image is then subtracted from the original one; diffuse background that has been little affected by the blurring is thus removed and only sharper features are preserved. An improved version of this approach, called nearest neighbours, utilises additional information present in a 3-dimensional image (a stack of images acquired for different axial positions of the focal plane) by subtracting from each image in the stack the blurred versions of its nearest neighbours, the images acquired at the adjacent planes below and above the image in question [168, 170]. These approaches and other ways of background subtraction such as the rolling ball algorithm, are very simple computationally and can deliver impressive-looking results; however, it should be remembered that they reduce the information content of the images rather than adding to it, potentially producing serious artefacts, and cannot be therefore considered in any way equivalent to hardware sectioning approaches [168].

Image deconvolution represents a more sophisticated, albeit more computationally intensive, approach to (not only) out-of-focus background removal from widefield images [168, 171, 172]. As the name suggests, deconvolution attempts to estimate what the image would look like if it has not been subject to convolution with the microscope PSF (see Sect. 3.1). Because of the axial extent of the PSF (which is considerably larger than its lateral extent) fluorophores in out-of-focus planes contribute to the image, producing blurry background. Using the knowledge of the PSF (which can be either predicted theoretically or characterised experimentally by imaging, for example small florescent beads), deconvolution can remove the contribution of the out-of-focus fluorophores. Similarly, deconvolution can also improve the contrast of small details in the image by reducing the blurring effects of the PSF in the lateral direction. As an example of such features, we can consider the two closely spaced lines in Fig. 2b, e which suffer from poor contrast because of the large overlap of the PSFs. In this way, deconvolution can effectively improve the image resolution and in this capacity, it is often applied even on images acquired with confocal microscopy and other microscopy modalities with optical sectioning capabilities [76, 171].

6 Resolution Beyond the Diffraction Limit

The resolution limit introduced in Sect. 3.1 applies to standard widefield optical microscopy without any a-priory assumptions about the specimen and, as Ernst Abbe himself noted in his seminal work on the topic, the limit does not necessarily apply under different experimental conditions [71, 73]. Since Abbe's times, various approaches to resolving structures finer than the diffraction limit have been explored. New technologies that became available in the second half of the twentieth century, particularly lasers and computers, enabled practical applications of such approaches, generally termed super-resolution microscopy, towards the end of the twentieth century [71]. This led to several ground-breaking papers published around the turn of the century, which greatly boosted the practical interest in super-resolution microscopy [173–181]. Since then, numerous new approaches have been proposed and many super-resolution techniques have become widely used and available in standard commercial microscopes. The field has become so broad, that this section can give only a very limited view of it; more information can be found in numerous reviews [182–187].

Super-resolution microscopy techniques circumvent the diffraction resolution limit by using usually one (or more) of these ingredients, which were not present in Abbe's theory: non-linear effects such as stimulated emission [173] or fluorescence saturation [188–190], assumptions of sparse fluorophore distribution [191–195], near-field optics [196–199] and quantum statistics of photons [199–203]. The above-mentioned fluorescence saturation is in general a problematic phenomenon in fluorescence microscopy. Because of the finite time spent by a fluorophore in the excited state before emitting a photon, the photon emission rate from a fluorophore is limited, regardless of the excitation intensity. At low excitation intensities, the fluorescence intensity grows approximately proportionally with increasing excitation intensity; however, at higher excitation intensities, the fluorescence intensity increase rate is lower than that of the excitation intensity, until it eventually completely saturates. Usually, excitation intensities in fluorescence microscopy are chosen to be safely below the saturation threshold since higher excitation intensities increase the risk of photodamage to the specimen without adequate increase in fluorescence signal. The use of fluorescence saturation for resolution enhancement demonstrates how otherwise problematic phenomena can be harnessed to enhance the capabilities of fluorescence microscopy.

The subsequent Sects. 6.1–6.5 introduce briefly the main branches of super-resolution microscopy with one notable exception, stimulated emission depletion microscopy (STED) and related techniques [173, 205–208]. Omission of this widespread and powerful super-resolution approach is explained by it being the topic of chapter "STED and RESOLFT Fluorescence Nanoscopy". Just very briefly, STED is a point-scanning super-resolution approach that can be implemented as a modification of a laser scanning confocal microscope. Excitation is provided by a diffraction-limited laser focus just like in a regular LSM; the difference lies in applying a second laser beam of longer wavelength, which induces stimulate emission of the

fluorophores. The second beam is specially shaped to have zero intensity in its centre (so-called doughnut beam profile); hence, fluorophores in the centre of the excitation volume do not undergo stimulated emission and remain in the excited state. The collected fluorescence, therefore, originates from a reduced, sub-diffraction, volume. Note that saturation of the stimulated emission is essential for reaching sub-diffraction resolution.

6.1 Near-Field Fluorescence Microscopy

The diffraction limit of resolution holds for far-field optical microscopy, assuming the aperture of the objective lens as well as the distance between the objective lens and the focal plane are many times larger than the wavelength of light. This assumption held for all the microscopy modalities described so far in this chapter. However, it is not the case for near-field fluorescence microscopy, using a sub-wavelength aperture to deliver excitation light to and/or collect the fluorescence of fluorophores at sub-wavelength distances from the aperture. The resolution is limited only by the aperture size in such a scenario. The aperture can be experimentally realised, for example by the end of a tapered optical fibre. Because of the requirement of the sub-diffraction distance between the aperture and the fluorophores, the technique is limited to imaging surface structures, such as cell membranes [196–198]. The image is then captured by scanning the aperture along the surface of interest, collecting fluorescence from a tiny, sub-wavelength surface area at a time. This approach, called near-field scanning optical microscopy (NSOM) can be, therefore, regarded as a form of scanning-probe microscopy, together with, for example AFM.

Evanescent fields employed in TIRF and SAF microscopies are another example of near-field optical phenomena employed in fluorescence microscopy and providing sub-wavelength optical sectioning, which can be seen as a form of axial super-resolution.

6.2 Single Molecule Localisation Microscopy (SMLM) and Fluorescence Fluctuation-Based Techniques

SMLM is a conceptually remarkably simple, yet very powerful, super-resolution strategy that does not require any specialised microscopy setup. A widefield microscope with a sensitive camera capable of single-molecule detection is all that is needed [60, 209, 210]; confocal or lightsheet implementations are also possible [211–213]. To explain its principle, let us first consider an image of a single fluorophore, which is, as we said in Sect. 3.1, the PSF centred at the geometrically perfect image of the fluorophore. By finding the centre of the respective PSF, we can

pinpoint the location of the fluorophore with, in principle, unlimited precision. In practice, the localisation precision is limited only by the signal-to-noise ratio of the image, not by the PSF width, and can reach nm order [214, 215], or even better if performed at cryogenic temperatures [216]. In this way, sparsely distributed fluorophores, separated ideally by distances much larger than the PSF width, can be imaged with deeply sub-diffraction resolution. However, such sparse fluorophore distributions are in general not sufficient for imaging arbitrary continuous structures. Nyquist-Shannon sampling theorem dictates that to resolve details as small as d, the structure needs to be labelled by fluorophores spaced not more than $d/2$ apart, unless of course a-priory assumptions about the structures can supplement the missing information. At such high fluorophore densities, it is, however, impossible to resolve PSFs corresponding to individual fluorophores and find their centres. The trick employed in SMLM to overcome this problem is illustrated in Fig. 9. If only a sparse subset of fluorophores is fluorescent at a time, positions of those fluorophores can be precisely localised. By acquiring a stack of many such images (frames), each providing a different random subset of fluorophore positions, we eventually accumulate enough fluorophore positions to resolve arbitrary structures with sub-diffraction resolution limited by the localisation precision of individual fluorophores.

This generic principle has various practical implementations differing in the ways how to ensure that only a sparse subset of fluorophores contributes to each frame. There exist two generic strategies, each with many variants varying in experimental details:

1. Employing transitions of fluorophores between a dark (non-fluorescent) and a bright (fluorescent) state. The fluorophores in this case are static, attached to the structure of interest being imaged. The original implementation of photoactivation localisation microscopy (PALM) used, for example, photoactivatable fluorescent protein molecules that reside initially mostly in a dark state from which they can be activated to a fluorescent state by UV light. With properly tuned intensity of the UV illumination, only a parse subset of fluorescent protein molecules is activated; the activated molecules are then imaged and, while doing so, irreversibly photobleached, allowing another sparse subset to be activated and imaged [176, 217]. Later, many new photoactivable fluorescent proteins have been introduced as well as photo-convertible fluorescent proteins (which change colour of their fluorescent emission upon, usually UV, illumination) and photo-switchable proteins, which can undergo repeated cycles of switching between bright and dark states [218–220]. Stochastic optical reconstruction microscopy (STORM), another example of this generic strategy, uses stochastic transitions between bright and dark states (referred to as blinking), exhibited by many organic fluorophores [175, 178, 221]. High excitation intensities and specific chemical environments are usually needed to induce suitable blinking dynamics [222, 223].
2. Employing transient binding of fluorophores to the structures of interest. The structure of interest is in this case not labelled by static fluorophores; rather, majority of fluorophores diffuse in the surrounding medium and only a small

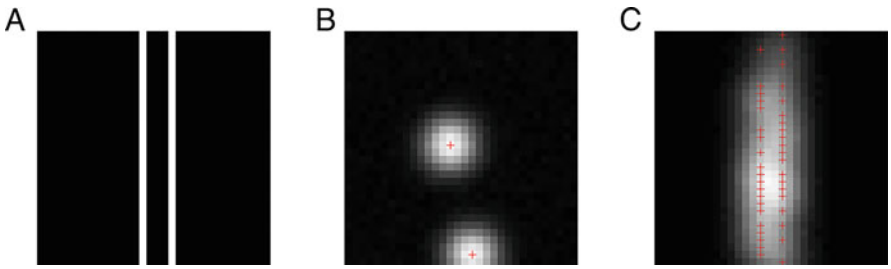

Fig. 9 An illustration of the principle of single molecule localisation microscopy (SMLM). The underlying structure consists of 2 thin fluorescently labelled parallel lines separated by the distance of 150 nm (**a**). When only a sparse subset of fluorophores emits light, the positions of those fluorophores can be localised with sub-diffraction accuracy as the centres of the respective PSFs (**b**). The last panel (**c**) shows an average of 100 such images, each containing the contribution from a random sparse subset of fluorophores. The average image has diffraction-limited resolution ($R_{PSF} = 339$ nm) and the two lines are unresolved; however, the overlayed fluorophore localisations from all of the 100 individual images (displayed as red crosses) clearly resolve the two lines. More localisations would be needed to unambiguously identify the structure as two parallel continuous lines unless the information contained in the image is supplemented by a-priori assumptions such as an expectation that the underlying structure consists of parallel continuous lines. The dimensions of the images are 1,600 × 1,600 nm. The PSF was for simplicity approximated by a Gaussian function

fraction of them binds to the structure of interest at a time. Non-bound fluorophores in the medium typically diffuse over long enough distances within the camera exposure time to make their images practically completely smeared out, thus preventing them from being localised. In each frame, a sparse pattern of fluorophores is visible, marking the positions of a sparse subset of possible binding sites. By accumulating the frames, increased number of binding sites is revealed, until the whole structure can be resolved [181, 224–226]. This approach is usually referred to as Points accumulation for imaging in nanoscale topography (PAINT). If the fluorescent molecules perform diffusive movement along the structure of interest, tracking their movement reveals simultaneously their dynamics as well as super-resolved details of the underlying structure (provided enough trajectories have been accumulated to cover the whole structure with sufficient density). This is the principle of a technique called single-particle tracking PALM (sptPALM) [227–230].

Note that the results of SMLM are not images, but rather sets of fluorophore coordinates (and other characteristics such as the amplitude and width of the respective PSF from which the fluorophore was localised). An image is generated from such data usually by convolution of the fluorophore localisations with a suitable narrow PSF, the width of which can be chosen to match the expected localisation precision [191, 231].

Figure 9 explicitly illustrates SMLM principle for localising fluorophores within the focal plane, thus achieving lateral super-resolution. However, SMLM can be extended to 3 dimensions by including axial localisation of the fluorophores with

sub-wavelength precision. Fluorophores in the focal plane can be recognised according to the width of the corresponding PSFs being the narrowest (diffraction limited). The further a fluorophore is from the focal plane, the broader is the respective PSF, until it eventually becomes smeared out to such an extent that localisation of the fluorophore becomes impossible [232]. However, for a well-corrected objective lens, the broadening of the PSF is symmetrical both below and above the focal plane; thus, analysing the PSF width identifies only the absolute axial distance, but not the direction of the fluorophore's position from the focal plane. This limitation can be overcome by modifying the PSF to have distinct shapes for fluorophores located above and below the focal plane, respectively. This is practically realised by introducing, for example astigmatic lenses or phase masks into the emission light path before the camera [233–236]. For astigmatic lenses, the accessible axial range is below 1 μm; for some phase masks, it can exceed 10 μm [233]. Other schemes for 3-deimensional SMLM involve simultaneous acquisition of images in multiple focal planes or interferometric approaches [237–240].

To achieve high degrees of sparsity, favourable for precise localisation of individual fluorophores, fluorophores either need to spend most of the time in the dark states or most of the binding sites need to be vacant at all times (in the cases when strategy 2 is used). This leads to the need of collecting high numbers of frames (often on the order of thousands) to accumulate enough localisations, translating to long acquisition times. Movement of any structures of interest within the prolonged acquisition time compromises the resolution, potentially negating the resolution enhancement, beside possibly producing a distorted image. This can be particularly problematic in live-cell SMLM [241]. Localisation algorithms able to process overlapping PSFs relax the requirements on fluorophore sparsity, and thus the time needed for SMLM data acquisition [242–244].

A further reduction in the image acquisition time, often by more than an order of magnitude, is achieved by related super-resolution techniques employing stochastic fluorophore blinking to enhance image resolution without depending on localising individual fluorophores [60, 194, 245–251]. These techniques are similar to SMLM in many aspects, such as the experimental implementation and structure of the raw image data, which also consist of time series of frames, each containing contributions from a subset of fluorophores. However, in contrast to SMLM, these techniques yield directly a super-resolved image rather than a list of fluorophore positions. For example, super-resolution optical fluctuation imaging (SOFI) uses temporal cumulants of fluorescence fluctuations to generate the super-resolved image. While these techniques still require fluorophore intensities to fluctuate, this does not have to be on/off blinking as required in SMLM; transitions between a brighter and a darker state are sufficient. Since individual fluorophores are not localised, the techniques can deal with higher fluorophore densities; however, SMLM in general reaches higher resolution enhancement.

6.3 Structured Illumination Microscopy (SIM)

SIM represents a very generic framework for super-resolution imaging. To understand its principle, it is very helpful to introduce the concept of spatial frequency and Fourier transform of images. Spatial-domain representation of images is what we usually imagine under the term "microscopy image", a representation of light intensity distribution as a function of spatial coordinates in 2 or 3 dimensions. The spatial-domain representation can be translated to frequency domain by Fourier transform. Frequency domain representation of an image is easily understood for an image of periodically repeating structures, which are described in frequency domain by the number of repetitions per a unit of distance. It can be shown mathematically that any arbitrary, non-periodic, structure can be described as a series of harmonic functions of different spatial frequencies. Frequencies approaching infinity are needed to describe sharp edges; hence the image is blurred by placing an upper limit on the spatial frequency bandwidth. The performance of an imaging system is described in frequency domain by its optical transfer function (OTF), which is a Fourier transform of its PSF. In a simplified approximation, the objective lens aperture can be described as a low-pass filter with cut-off frequency of $f_d = 1/d$, where d is the spatial-domain resolution limit. Increasing image resolution is thus equivalent to increasing its high-frequency content.

In the traditional implementation of SIM [174], the specimen is excited by a periodic pattern of bright and dark stripes (generated for example by placing a diffraction grating into the excitation light path) at spatial frequency f_x, resulting in spatial modulation of fluorophore excitation efficiency. The fluorescence image is then determined by the distribution of fluorophores in the specimen as well as by the periodic excitation light modulation. This can be described in the frequency domain as interference of the spatial frequency f_x of the periodic excitation pattern with spatial frequencies describing fluorescent structures in the specimen, analogously to describing interference of electromagnetic or acoustic waves. Interference of two waves produces waves with frequencies equal to the sum and the difference between the frequencies of the individual waves. Let us consider a spatial frequency f_s associated with sub-diffraction structural details of the specimen. Such frequency is not present in a diffraction-limited image as it is outside of the bandwidth supported by the objective lens ($f_s > f_d$). However, if the differential frequency $f_s - f_x$ lies within the supported bandwidth, such structural details can be reconstructed from an image acquired with spatially modulated excitation. Since the excitation in epifluorescence microscopy is delivered by the same objective lens, the modulation frequency of the excitation light needs to be within the objective's bandwidth ($f_x \leq f_d$), leading to the following observation about f_s:

$$f_s - f_x \leq f_d$$
$$f_s \leq 2 f_d$$

In other words, the maximum resolution enhancement of the traditional SIM implementation does not exceed factor of 2.

Multiple images for different positions and orientations of the excitation intensity are needed to generate a single super-resolved SIM image. The pattern needs to be shifted in space to ensure that every point in the field of view has been exposed to (sufficiently high) excitation intensity and rotated to ensure resolution is enhanced for arbitrarily oriented structures. The traditional SIM implementation uses at least 9 images (3 shifts for 3 rotations) to produce a super-resolved image; SIM reconstruction algorithms that can work with as few as 7 or 6 images have been also proposed [252, 253]. The modest numbers of images required compared to SMLM make SIM better suited for observing dynamical processes in living specimens. For the best SIM results, it is advisable to acquire images at multiple focal planes and use the 3-dimensional information in SIM reconstruction. Multifocal and lightsheet implementations of SIM for 3-dimensional imaging have been also described [254–256].

The traditional SIM reconstruction algorithm assumes the knowledge of the excitation patterns. This makes it sensitive to specimen-induced optical aberrations that tend to distort the excitation patterns. This issue is alleviated by blind reconstruction algorithms for SIM, which do not require any knowledge of the excitation patterns, making them applicable to the case of random excitation patterns as well [257–263].

Resolution enhancement exceeding factor of 2 can be achieved in SIM by harnessing non-linear optical effects [264, 265] such as fluorescence saturation [190]. Although the illumination pattern does not contain spatial frequencies exceeding f_d, the non-linear relationship between excitation and emission intensities results in higher frequency components being modulated on the fluorescence emission distribution. However, the high excitation intensities needed to produce significant florescence saturation can be harmful to living specimens.

The 2-times limit on resolution enhancement can be also circumvented if the illumination pattern does not have to be transmitted by the microscope objective [266–268]. Strategies employing photonic chips, surface plasmons or hyperbolic metamaterials to generate patterned illumination increase considerably the resolution enhancement without the need for a highly specialised microscopy setup [269–274]; their main limitation is the shallow penetration depth resulting from the use of near-field optical phenomena in generating the patterned excitation intensity distribution.

6.4 Confocal Microscopy and Related Approaches

As mentioned in Sect. 4, reducing the size of the confocal aperture below 1 AU improves the resolution of confocal microscopy achieving sub-diffraction resolution. The resolution enhancement, however, comes at the cost of reduced signal. Consequently, this approach is not widely used in biological fluorescence microscopy which often struggles against limited photon budget. Resolution improvement

without the sacrifice of signal can be achieved in laser scanning microscopy by replacing the confocal aperture and a point detector with a spatially resolved detector, such as a camera or a detector array [87, 89, 202, 275–281]. The whole camera or detector array captures all signal available, while a single camera pixel or a single detector in the array acts as a small pinhole (smaller than 1 AU). The distribution of the signal across individual pixels or individual detectors, thus, provides information allowing computational reconstruction of a super-resolved image, for example by an algorithm termed pixel reassignment. The resolution enhancement is similar to standard SIM, that means approaching factor of 2. The principle of pixel reassignment can be also realised in a hardware version, termed photon reassignment then, employing an additional beam scanning step that sweeps the emission beam across the camera with a twice as large sweep (to match the resolution doubling) as the sweep of the scanner used to scan the laser focus across the specimen [88, 282–284]. This approach is usually termed re-scan confocal microscopy. In multifocal or spinning disk versions, an additional 2x magnifying microlens array is added to the emission path [285–287].

While approaches derived from confocal microscopy evolved from a different starting point than SIM, they are closely related. Both use sparse distributions of excitation intensity and generate a single super-resolved image from signal captured with series of different excitation intensity distributions (which together make sure that every point within the field of view has been exposed to excitation). Considering this similarity, all these techniques can be viewed as variants of a generalised SIM approach [71, 187, 192, 286–291].

6.5 Computational Approaches

Computational super-resolution methods, that can be applied as a post-processing step to an image acquired with any standard microscopy modality, are very attractive for their flexibility, absence of special experimental requirements and, consequently, affordability. Since a super-resolved image has higher information contents than a diffraction-limited image, the additional information needs to be derived from a-priori knowledge or assumptions. For example, image deconvolution uses the knowledge of microscope PSF (either determined experimentally or predicted theoretically based on the parameters of the microscope) to increase the image resolution by factors potentially exceeding 2, although in practice, the resolution enhancement is usually much more modest because of limited signal to noise ratio [205, 288, 289, 292]. Deconvolution delivers the best results if applied to a 3-dimensional image stack, in which case it can benefit from the knowledge of the PSF in all three dimensions. Therefore, 3-dimensional stacks are usually acquired for deconvolution processing even if just a single plane is of interest; the additional planes can be viewed as an additional source of information used in generating a super-resolved image of the plane of interest.

Techniques based on deep learning represent an attractive alternative to traditional deconvolution algorithms, which they can outperform in terms of computational speed as well as resolution enhancement [293]. They can be trained on sets of image pairs consisting each of a synthetic ground-truth image and the same image degraded by simulated microscope imaging (considering PSF and noise). The training process thus supplies a-priori knowledge about the microscope PSF as well as about the types of structures expected in the specimen (through the types of structures present in the synthetic training images). Although assumptions about PSF are used in the training process, the technique is much less sensitive to the actual PSF than traditional deconvolution algorithms, making it applicable even in cases where the details of the microscope PSF are not known [293].

Some computational techniques perform optimally only on images with a sufficient degree of sparsity in fluorescence intensity distribution (which is, however, hugely lower than the high degrees of sparsity required by SMLM) [193, 195]. This is a reasonable assumption in fluorescence microscopy where most images exhibit such levels of sparsity (featuring, for example small fluorescent puncta or filamentous fluorescent structures). Examples of such techniques include super-resolution radial fluctuations (SRRF) employing local gradient fields convergence (termed radiality) [294, 295] or mean-shift super-resolution (MSSR) employing mean-shift theory [296] to enhance image resolution. While both techniques are able to increase the resolution of individual images, their resolution enhancement is significantly increased if time series of images are available. The fluorescence intensity fluctuations captured in the time series provide additional information that can be converted to resolution enhancement. This links these powerful techniques to fluctuation-based approaches such as SOFI introduced in Sect. 6.2; however, their reduced dependence on intensity fluctuations makes them significantly more flexible and usable under a broader range of conditions [193, 294].

Sparsity in fluorescence images, beneficial for the performance of many computational super-resolution approaches, can be enhanced by a sparse distribution of excitation light [192, 288]. If sparse excitation distributions are used instead of homogeneous excitation, multiple images with different excitation distributions need to be captured sequentially to ensure that every point within the field of view has been exposed to excitation. Super-resolution techniques employing such a mode of excitation can be viewed as examples of generalised SIM (together with confocal approaches, see Sects. 6.3 and 6.4).

7 Concluding Remarks and Outlook

Because of its ubiquitous use in, not only, biological and biomedical sciences, fluorescence microscopy has developed into such a broad field that this chapter could provide only a very basic introduction which necessarily missed many important aspects of the topic and many noteworthy developments. Many of the more

specialised topics can be found in other chapters of this volume, to which this chapter can serve as an introduction.

A very important topic that has been mostly avoided in this chapter is processing and analysis of microscopy images. An introduction to this topic can be found, for example in references [169, 297, 298]. Segmentation, identification of the objects of interest, represents a critical step in many image analysis workflows such as object counting, object tracking, object morphometry or object-based colocalisation analysis. This step is often relatively simple in fluorescence microscopy compared to other techniques such as brightfield or scanning electron microscopy. Since the objects of interest typically appear bright against dark background, a single global threshold is often enough to distinguish pixels belonging to the objects of interest from background pixels and simple global thresholding algorithm can be applied successfully in such cases [299, 300]. More challenging scenarios involving uneven background and/or uneven intensity distribution in the objects of interest require more complex segmentation approaches such as locally determined thresholds or increasingly popular deep-learning approaches [301, 302].

Deep learning is also very powerful in enhancing image quality, outperforming traditional deconvolution algorithms in terms of speed as well as image improvement [293, 303]. This is an example of a trend where the advances in computational power and image processing algorithms relax the requirements on the microscope hardware, sample preparation and on acquisition time, allowing obtaining images of comparable quality with simpler microscope setups and/or in a shorter time. The lower cost of increasing computational capacity compared to upgrading highly specialised microscopy hardware is another aspect of this trend, which has the potential of making high-performance fluorescence microscopy more affordable and widespread. All of this is particularly pronounced in the case of lens-free microscopy, which uses remarkably simple and cost-effective setups combined with computational image reconstruction. While lens-free microscopy has been mostly limited to transmitted light imaging, there have been also lens-free implementations of fluorescence microscopy [27–32].

Another obvious trend in fluorescence microscopy has been the increasing throughput of, especially 3-dimensional, imaging, driven by advances in lightsheet microscopy and digital camera technology. Increasingly larger specimen volumes can be imaged in shorter time and at higher resolution. At the same time, fluorescence microscopy tends to be gentler and less invasive to allow observation of living specimens for longer periods and under less artificial conditions as demonstrated, for example, by fluorescence micro-endoscopy or miniature head-mounted microscopes for brain imaging in freely moving rodents [304, 305]. The increasing size of the 3-dimensional datasets and the growing rate at which they are produced place high demands not only on the computational power needed for their real-time processing but also on data storage capacity required to keep them. To tackle the latter challenge, solutions have been proposed to reduce the size of the dataset while keeping all relevant information contents [306–308]. Such solutions may prove critical to sustaining the current trends in fluorescence microscopy in the long run [309].

References

1. Robertson J, McGoverin C, Vanholsbeeck F, Swift S (2019) Optimisation of the protocol for the LIVE/DEAD® BacLightTM bacterial viability kit for rapid determination of bacterial load. Front Microbiol 10:801. https://doi.org/10.3389/fmicb.2019.00801
2. Baddeley D, Bewersdorf J (2018) Biological insight from super-resolution microscopy: what we can learn from localization-based images. Annu Rev Biochem 87(1):965. https://doi.org/10.1146/annurev-biochem-060815-014801
3. Ishikawa-Ankerhold HC, Ankerhold R, Drummen GPC (2012) Advanced fluorescence microscopy techniques--FRAP, FLIP, FLAP, FRET and FLIM. Molecules 17(4): 4047–4132. https://doi.org/10.3390/molecules17044047
4. Wang Y, Schellenberg H, Walhorn V, Toensing K, Anselmetti D (2017) Binding mechanism of fluorescent dyes to DNA characterized by magnetic tweezers. Mater Today Proc 4:S218–S225. https://doi.org/10.1016/j.matpr.2017.09.190
5. Otto F, Tsou KC (1985) A comparative study of DAPI, DIPI, and Hoechst 33258 and 33342 as chromosomal DNA stains. Stain Technol 60(1):7–11. https://doi.org/10.3109/10520298509113885
6. Pagano RE, Ozato K, Ruysschaert J-M (1977) Intracellular distribution of lipophilic fluorescent probes in mammalian cells. Biochim Biophys Acta Biomembr 465(3):661–666. https://doi.org/10.1016/0005-2736(77)90282-6
7. Greenspan P, Mayer EP, Fowler SD (1985) Nile red: a selective fluorescent stain for intracellular lipid droplets. J Cell Biol 100(3):965–973. https://doi.org/10.1083/jcb.100.3.965
8. Horisawa K (2014) Specific and quantitative labeling of biomolecules using click chemistry. Front Physiol 5:457. https://doi.org/10.3389/fphys.2014.00457
9. Yan Q, Bruchez MP (2015) Advances in chemical labeling of proteins in living cells. Cell Tissue Res 360(1):179–194. https://doi.org/10.1007/s00441-015-2145-4
10. Thorn K (2017) Genetically encoded fluorescent tags. Mol Biol Cell 28(7):848–857. https://doi.org/10.1091/mbc.e16-07-0504
11. Schaefer PM, Kalinina S, Rueck A, von Arnim CAF, von Einem B (2019) NADH autofluorescence – a marker on its way to boost bioenergetic research. Cytom Part A 95(1): 34–46. https://doi.org/10.1002/cyto.a.23597
12. Oxborough K (2004) Imaging of chlorophyll a fluorescence: theoretical and practical aspects of an emerging technique for the monitoring of photosynthetic performance. J Exp Bot 55(400):1195–1205. https://doi.org/10.1093/jxb/erh145
13. Bolte S, Cordelières FP (2006) A guided tour into subcellular colocalization analysis in light microscopy. J Microsc 224(3):213–232. https://doi.org/10.1111/j.1365-2818.2006.01706.x
14. Adler J, Parmryd I (2010) Quantifying colocalization by correlation: the Pearson correlation coefficient is superior to the Mander's overlap coefficient. Cytom Part A 77(8):733–742. https://doi.org/10.1002/cyto.a.20896
15. Dunn KW, Kamocka MM, McDonald JH (2011) A practical guide to evaluating colocalization in biological microscopy. Am J Physiol Physiol 300(4):C723–C742. https://doi.org/10.1152/ajpcell.00462.2010
16. Valm AM, Oldenbourg R, Borisy GG (2016) Multiplexed spectral imaging of 120 different fluorescent labels. PLoS One 11(7):e0158495
17. Klymchenko AS (2017) Solvatochromic and fluorogenic dyes as environment-sensitive probes: design and biological applications. Acc Chem Res 50(2):366–375. https://doi.org/10.1021/acs.accounts.6b00517
18. Han J, Burgess K (2010) Fluorescent indicators for intracellular pH. Chem Rev 110(5): 2709–2728. https://doi.org/10.1021/cr900249z
19. Zhang X-X, Wang Z, Yue X, Ma Y, Kiesewetter DO, Chen X (2013) pH-sensitive fluorescent dyes: are they really pH-sensitive in cells? Mol Pharm 10(5):1910–1917. https://doi.org/10.1021/mp3006903

20. Palonpon AF et al (2013) Raman and SERS microscopy for molecular imaging of live cells. Nat Protoc 8(4):677–692. https://doi.org/10.1038/nprot.2013.030
21. Gritti N, Kienle S, Filina O, van Zon JS (2016) Long-term time-lapse microscopy of C. elegans post-embryonic development. Nat Commun 7(1):12500. https://doi.org/10.1038/ncomms12500
22. Kamei M, Weinstein BM (2005) Long-term time-lapse fluorescence imaging of developing zebrafish. Zebrafish 2(2):113–123. https://doi.org/10.1089/zeb.2005.2.113
23. Collins JT et al (2020) Robotic microscopy for everyone: the OpenFlexure microscope. Biomed Opt Express 11(5):2447. https://doi.org/10.1364/boe.385729
24. Merces GOT, Kennedy C, Lenoci B, Reynaud EG, Burke N, Pickering M (2021) The incubot: a 3D printer-based microscope for long-term live cell imaging within a tissue culture incubator. HardwareX 9. https://doi.org/10.1016/j.ohx.2021.e00189
25. Ishmukhametov RR, Russell AN, Wheeler RJ, Nord AL, Berry RM (2016) A simple low-cost device enables four epi-illumination techniques on standard light microscopes. Sci Rep 6 (February):1–13. https://doi.org/10.1038/srep20729
26. Stewart C, Giannini J (2016) Inexpensive, open source epifluorescence microscopes. J Chem Educ 93(7):1310–1315. https://doi.org/10.1021/acs.jchemed.5b00984
27. Coskun AF, Sencan I, Su T-W, Ozcan A (2010) Lensless wide-field fluorescent imaging on a chip using compressive decoding of sparse objects. Opt Express 18(10):10510. https://doi.org/10.1364/oe.18.010510
28. Pang S, Han C, Kato M, Sternberg PW, Yang C (2012) Wide and scalable field-of-view Talbot-grid-based fluorescence microscopy. Opt Lett 37(23):5018. https://doi.org/10.1364/ol.37.005018
29. Banik S et al (2021) Recent trends in smartphone-based detection for biomedical applications: a review. Anal Bioanal Chem:2389–2406
30. Kuo G, Linda Liu F, Grossrubatscher I, Ng R, Waller L (2020) On-chip fluorescence microscopy with a random microlens diffuser. Opt Express 28(6):8384. https://doi.org/10.1364/oe.382055
31. Sasagawa K, Kimura A, Haruta M, Noda T, Tokuda T, Ohta J (2018) Highly sensitive lens-free fluorescence imaging device enabled by a complementary combination of interference and absorption filters. Biomed Opt Express 9(9):4329. https://doi.org/10.1364/boe.9.004329
32. Shanmugam A, Salthouse CD (2014) Lensless fluorescence imaging with height calculation. J Biomed Opt 19(01):1. https://doi.org/10.1117/1.jbo.19.1.016002
33. Sandoz PA, Tremblay C, van der Goot FG, Frechin M (2019) Image-based analysis of living mammalian cells using label-free 3D refractive index maps reveals new organelle dynamics and dry mass flux. PLoS Biol 17(12):e3000553
34. Elsayad K et al (2016) Mapping the subcellular mechanical properties of live cells in tissues with fluorescence emission-Brillouin imaging. Sci Signal 9(435):rs5. https://doi.org/10.1126/scisignal.aaf6326
35. Clayton AHA, Hanley QS, Arndt-Jovin DJ, Subramaniam V, Jovin TM (2002) Dynamic fluorescence anisotropy imaging microscopy in the frequency domain (rFLIM). Biophys J 83(3):1631–1649. https://doi.org/10.1016/S0006-3495(02)73932-5
36. Suhling K, Levitt J, Chung P-H (2014) Time-resolved fluorescence anisotropy imaging. Methods Mol Biol 1076:503–519. https://doi.org/10.1007/978-1-62703-649-8_22
37. Timr Š et al (2014) Accurate determination of the orientational distribution of a fluorescent molecule in a phospholipid membrane. J Phys Chem B 118(4):855–863. https://doi.org/10.1021/jp4067026
38. Ladouceur A-M, Brown CM (2021) Fluorescence microscopy light source review. Curr Protoc 1(9):e243. https://doi.org/10.1002/cpz1.243
39. Mubaid F et al (2019) Fluorescence microscope light source stability. Histochem Cell Biol 151(4):357–366. https://doi.org/10.1007/s00418-019-01776-6
40. Heřman P, Maliwal B, Lin H, Lakowicz J (2001) Frequency domain microscopy with the LED as a light source. J Microsc 203:176–181. https://doi.org/10.1046/j.1365-2818.2001.00943.x

41. Bei L, Dennis GI, Miller HM, Spaine TW, Carnahan JW (2004) Acousto-optic tunable filters: fundamentals and applications as applied to chemical analysis techniques. Prog Quantum Electron 28(2):67–87. https://doi.org/10.1016/S0079-6727(03)00083-1
42. Birk H, Engelhardt J, Storz R, Hartmann N, Bradl J, Ulrich H (2002) Programmable beam-splitter for confocal laser scanning microscopy. Proc SPIE 4621
43. Parasassi T, De Stasio G, d'Ubaldo A, Gratton E (1990) Phase fluctuation in phospholipid membranes revealed by Laurdan fluorescence. Biophys J 57(6):1179–1186. https://doi.org/10.1016/S0006-3495(90)82637-0
44. Yavas S, Macháň R, Wohland T (2016) The epidermal growth factor receptor forms location-dependent complexes in resting cells. Biophys J 111(10). https://doi.org/10.1016/j.bpj.2016.09.049
45. Lambert TJ (2019) FPbase: a community-editable fluorescent protein database. Nat Methods 16(4):277–278. https://doi.org/10.1038/s41592-019-0352-8
46. Jiménez-Sánchez D, Ariz M, Morgado JM, Cortés-Domínguez I, Ortiz-de-Solórzano C (2020) NMF-RI: blind spectral unmixing of highly mixed multispectral flow and image cytometry data. Bioinformatics 36(5):1590–1598. https://doi.org/10.1093/bioinformatics/btz751
47. McRae TD, Oleksyn D, Miller J, Gao Y-R (2019) Robust blind spectral unmixing for fluorescence microscopy using unsupervised learning. PLoS One 14(12):e0225410
48. Bayer B (1976) Patent US3971065A, color imaging array, US3971065A
49. Janesick JR (2001) Scientific charge-coupled devices. SPIE Press, Bellingham
50. Stuurman N, Vale RD (2016) Impact of new camera technologies on discoveries in cell biology. Biol Bull 231(1):5–13. https://doi.org/10.1086/689587
51. Okten Z, Churchman LS, Rock RS, Spudich JA (2004) Myosin VI walks hand-over-hand along actin. Nat Struct Mol Biol 11(9):884–887. https://doi.org/10.1038/nsmb815
52. Namiki S, Ikegaya Y (2009) Current application and technology of functional multineuron calcium imaging. Biol Pharm Bull 32(1):1–9. https://doi.org/10.1248/bpb.32.1
53. Unruh JR, Gratton E (2008) Analysis of molecular concentration and brightness from fluorescence fluctuation data with an electron multiplied CCD camera. Biophys J 95(11):5385–5398. https://doi.org/10.1529/biophysj.108.130310
54. Bag N, Sankaran J, Paul A, Kraut RS, Wohland T (2012) Calibration and limits of camera-based fluorescence correlation spectroscopy: a supported lipid bilayer study. ChemPhysChem 13(11):2784–2794. https://doi.org/10.1002/cphc.201200032
55. Fossum ER (1993) Active pixel sensors: are CCDs dinosaurs? Proc SPIE 1900. https://doi.org/10.1117/12.148585
56. Beier HT, Ibey BL (2014) Experimental comparison of the high-speed imaging performance of an EM-CCD and sCMOS camera in a dynamic live-cell imaging test case. PLoS One 9(1). https://doi.org/10.1371/journal.pone.0084614
57. Singh AP et al (2013) The performance of 2D array detectors for light sheet based fluorescence correlation spectroscopy. Opt Express 21(7):8652–8668. https://doi.org/10.1364/OE.21.008652
58. Diekmann R, Till K, Müller M, Simonis M, Schüttpelz M, Huser T (2017) Characterization of an industry-grade CMOS camera well suited for single molecule localization microscopy – high performance super-resolution at low cost. Sci Rep 7(1):1–10. https://doi.org/10.1038/s41598-017-14762-6
59. Mandracchia B, Hua X, Guo C, Son J, Urner T, Jia S (2020) Fast and accurate sCMOS noise correction for fluorescence microscopy. Nat Commun 11(1):1–12. https://doi.org/10.1038/s41467-019-13841-8
60. Diederich B et al (2020) Nanoscopy on the Chea(i)p. bioRxiv. https://doi.org/10.1101/2020.09.04.283085
61. Chao J, Ram S, Ward ES, Ober RJ (2009) A 3D resolution measure for optical microscopy. Proc IEEE Int Symp Biomed Imaging 5193252:1115. https://doi.org/10.1109/ISBI.2009.5193252

62. Nieuwenhuizen RPJ et al (2013) Measuring image resolution in optical nanoscopy. Nat Methods 10(6):557–562. https://doi.org/10.1038/nmeth.2448
63. Banterle N, Bui KH, Lemke EA, Beck M (2013) Fourier ring correlation as a resolution criterion for super-resolution microscopy. J Struct Biol 183(3):363–367. https://doi.org/10.1016/j.jsb.2013.05.004
64. Barentine AES, Schroeder LK, Graff M, Baddeley D, Bewersdorf J (2018) Simultaneously measuring image features and resolution in live-cell STED images. Biophys J 115(6):951–956. https://doi.org/10.1016/j.bpj.2018.07.028
65. Tortarolo G, Castello M, Diaspro A, Koho S, Vicidomini G (2018) Evaluating image resolution in stimulated emission depletion microscopy. Optica 5(1):32. https://doi.org/10.1364/optica.5.000032
66. Raab M et al (2018) Using DNA origami nanorulers as traceable distance measurement standards and nanoscopic benchmark structures. Sci Rep 8(1):5–13. https://doi.org/10.1038/s41598-018-19905-x
67. Lin R, Clowsley AH, Lutz T, Baddeley D, Soeller C (2019) 3D super-resolution microscopy performance and quantitative analysis assessment using DNA-PAINT and DNA origami test samples. Methods 174:56–71. https://doi.org/10.1016/j.ymeth.2019.05.018
68. Thevathasan JV et al (2019) Nuclear pores as versatile reference standards for quantitative superresolution microscopy. Nat Methods 16(10):1045–1053. https://doi.org/10.1038/s41592-019-0574-9
69. Descloux A et al (2018) Combined multi-plane phase retrieval and super-resolution optical fluctuation imaging for 4D cell microscopy. Nat Photonics 12(3). https://doi.org/10.1038/s41566-018-0109-4
70. Pilger C et al (2021) Super-resolution fluorescence microscopy by line-scanning with an unmodified two-photon microscope. Philos Trans R Soc A Math Phys Eng Sci 379(2199). https://doi.org/10.1098/rsta.2020.0300
71. Cremer C, Masters BR (2013) Resolution enhancement techniques in microscopy. Eur Phys J H 38(3):281–344. https://doi.org/10.1140/epjh/e2012-20060-1
72. Kubitscheck U (2013) Principles of light microscopy. In: Kubitscheck U (ed) Fluorescence microscopy: from principles to biological applications1st edn. Wiley-VCH, Weinheim
73. Abbe E (1873) Beiträge zur Theorie des Mikroskops und der mikroskopischen Wahrnehmung. Arch für Mikroskopische Anat 9(1):413–468. https://doi.org/10.1007/BF02956173
74. Zhang Y, Gross H (2019) Systematic design of microscope objectives. Part I: system review and analysis. Adv Opt Technol 8(5):313–347
75. Diel EE, Lichtman JW, Richardson DS (2020) Tutorial: avoiding and correcting sample-induced spherical aberration artifacts in 3D fluorescence microscopy. Nat Protoc 15(9):2773–2784. https://doi.org/10.1038/s41596-020-0360-2
76. Lam F, Cladière D, Guillaume C, Wassmann K, Bolte S (2019) Super-resolution for everybody: an image processing workflow to obtain high-resolution images with a standard confocal microscope. Methods 115:17–27. https://doi.org/10.1016/j.ymeth.2016.11.003
77. Ji N (2017) Adaptive optical fluorescence microscopy. Nat Methods 14(4):374–380. https://doi.org/10.1038/nmeth.4218
78. Rodríguez C, Ji N (2018) Adaptive optical microscopy for neurobiology. Curr Opin Neurobiol 50:83–91. https://doi.org/10.1016/j.conb.2018.01.011
79. Sahu P, Mazumder N (2020) Advances in adaptive optics–based two-photon fluorescence microscopy for brain imaging. Lasers Med Sci 35(2):317–328. https://doi.org/10.1007/s10103-019-02908-z
80. Gallagher J, Delon A, Moreau P, Wang I (2017) Optimizing the metric in sensorless adaptive optical microscopy with fluorescence fluctuations. Opt Express 25(13):15558. https://doi.org/10.1364/oe.25.015558
81. Hell SW, Stelzer EH, Lindek S, Cremer C (1994) Confocal microscopy with an increased detection aperture: type-B 4Pi confocal microscopy. Opt Lett 19(3):222. https://doi.org/10.1364/ol.19.000222

82. Hell S, Stelzer EHK (1992) Properties of a 4Pi confocal fluorescence microscope. J Opt Soc Am A 9(12):2159–2166. https://doi.org/10.1364/JOSAA.9.002159
83. Antolovic IM, Bruschini C, Charbon E (2018) Dynamic range extension for photon counting arrays. Opt Express 26(17):22234–22248. https://doi.org/10.1364/OE.26.022234
84. Modi MN, Daie K, Turner GC, Podgorski K (2019) Two-photon imaging with silicon photomultipliers. Opt Express 27(24):35830–35841. https://doi.org/10.1364/OE.27.035830
85. Ching-Roa VD, Olson EM, Ibrahim SF, Torres R, Giacomelli MG (2021) Ultrahigh-speed point scanning two-photon microscopy using high dynamic range silicon photomultipliers. Sci Rep 11(1):1–12. https://doi.org/10.1038/s41598-021-84522-0
86. Caccia M, Nardo L, Santoro R, Schaffhauser D (2018) Silicon photomultipliers and SPAD imagers in biophotonics: advances and perspectives. Nucl Instruments Methods Phys Res Sect A Accel Spectrometers Detect Assoc Equip 926:101–117. https://doi.org/10.1016/j.nima.2018.10.204
87. Huff J (2015) The Airyscan detector from ZEISS: confocal imaging with improved signal-to-noise ratio and super-resolution. Nat Methods 12(12):i–ii. https://doi.org/10.1038/nmeth.f.388
88. De Luca GMR et al (2013) Re-scan confocal microscopy: scanning twice for better resolution. Biomed Opt Express 4(11):2644. https://doi.org/10.1364/boe.4.002644
89. Sheppard CJR et al (2020) Pixel reassignment in image scanning microscopy: a re-evaluation. J Opt Soc Am A 37(1):154–162. https://doi.org/10.1364/JOSAA.37.000154
90. Ilev IK, Waynant RW (2000) A simple submicron confocal microscope with a fiberoptic output. Rev Sci Instrum 71(11):4161–4164. https://doi.org/10.1063/1.1322589
91. Becker W et al (2016) A wide-field TCSPC FLIM system based on an MCP PMT with a delay-line anode. Rev Sci Instrum 87(9). https://doi.org/10.1063/1.4962864
92. Webb SED et al (2002) A wide-field time-domain fluorescence lifetime imaging microscope with optical sectioning. Rev Sci Instrum 73(4):1898–1907. https://doi.org/10.1063/1.1458061
93. Tisler J et al (2009) Fluorescence and spin properties of defects in single digit nanodiamonds. ACS Nano 3(7):1959–1965. https://doi.org/10.1021/nn9003617
94. Amos WB, White JG (2003) How the confocal laser scanning microscope entered biological research. Biol Cell 95(6):335–342. https://doi.org/10.1016/S0248-4900(03)00078-9
95. Borlinghaus RT (2006) MRT letter: high speed scanning has the potential to increase fluorescence yield and to reduce photobleaching. Microsc Res Tech 69(9):689–692. https://doi.org/10.1002/jemt.20363
96. Sheppard CJR, Mao XQ (1988) Confocal microscopes with slit apertures. J Mod Opt 35(7):1169–1185. https://doi.org/10.1080/09500348814551251
97. Kim S et al (2015) Spectrally encoded slit confocal microscopy using a wavelength-swept laser. J Biomed Opt 20(3):1–5. https://doi.org/10.1117/1.JBO.20.3.036016
98. Lee J, Miyanaga Y, Ueda M, Hohng S (2012) Video-rate confocal microscopy for single-molecule imaging in live cells and superresolution fluorescence imaging. Biophys J 103(8):1691–1697. https://doi.org/10.1016/j.bpj.2012.09.014
99. Amos WB, White JG (1995) Pawley JB (ed) Direct view confocal imaging systems using a slit aperture BT – handbook of biological confocal microscopy. Springer, Boston, pp 403–415
100. Chong SP, Pant S, Chen N (2011) Line-scan focal modulation microscopy for rapid imaging of thick biological specimens. Opt Sens Biophotonics:83111C. https://doi.org/10.1364/ACP.2011.83111C
101. Gräf R, Rietdorf J, Zimmermann T (2005) Live cell spinning disk microscopy. In: Rietdorf J (ed) Microscopy techniques. Springer, Berlin, pp 57–75
102. Halpern AR, Lee MY, Howard MD, Woodworth MA, Nicovich PR, Vaughan JC (2022) Versatile, do-it-yourself, low-cost spinning disk confocal microscope. Biomed Opt Express 13(2):1102–1120. https://doi.org/10.1364/BOE.442087
103. Petráň M, Hadravský M, Egger MD, Galambos R (1968) Tandem-scanning reflected-light microscope. J Opt Soc Am 58(5):661–664. https://doi.org/10.1364/JOSA.58.000661
104. Egger MD, Petráň M (1967) New reflected-light microscope for viewing unstained brain and ganglion cells. Science 157(3786):305–307. https://doi.org/10.1126/science.157.3786.305

105. Borlinghaus R, Gröbler B (1998) Basic principles and applications of confocal laser scanning microscopy. In: Isenberg G (ed) Modern optics, electronics and high precision techniques in cell biology. Springer, Berlin, pp 33–53
106. Kang SY, Duocastella M, Arnold CB (2020) Variable optical elements for fast focus control. Nat Photonics 14(9):533–542. https://doi.org/10.1038/s41566-020-0684-z
107. Deguchi T, Bianchini P, Palazzolo G, Oneto M, Diaspro A, Duocastella M (2020) Volumetric Lissajous confocal microscopy with tunable spatiotemporal resolution. Biomed Opt Express 11(11):6293. https://doi.org/10.1364/boe.400777
108. Lee D-R, Kim Y-D, Gweon D-G, Yoo H (2013) Dual-detection confocal fluorescence microscopy: fluorescence axial imaging without axial scanning. Opt Express 21(15):17839. https://doi.org/10.1364/oe.21.017839
109. Badon A et al (2019) Video-rate large-scale imaging with multi-Z confocal microscopy. Optica 6(4):389. https://doi.org/10.1364/optica.6.000389
110. He K et al (2018) Computational multifocal microscopy. Biomed Opt Express 9(12):6477. https://doi.org/10.1364/boe.9.006477
111. Tuchin EA, Zhu VV, Genina D (2022) Handbook of tissue optical clearing: new prospects in optical imaging.1st edn. CRC Press, Boca Raton
112. Zubkovs V et al (2018) Spinning-disc confocal microscopy in the second near-infrared window (NIR-II). Sci Rep 8(1):13770. https://doi.org/10.1038/s41598-018-31928-y
113. Sun C, Wang Y, Zhang H, Qian J (2017) Near-infrared laser scanning confocal microscopy and its application in bioimaging. Opt Quant Electron 50(1):35. https://doi.org/10.1007/s11082-017-1309-8
114. Xia F et al (2021) Short-wave infrared confocal fluorescence imaging of deep mouse brain with a superconducting nanowire single-photon detector. ACS Photonics 8(9):2800–2810. https://doi.org/10.1021/acsphotonics.1c01018
115. Wang M, Chen N (2019) Three-dimensional cellular imaging in thick biological tissue with confocal detection of one-photon fluorescence in the near-infrared II window. J Biophotonics 12(7):e201800459. https://doi.org/10.1002/jbio.201800459
116. Zhang Y et al (2021) Instant FLIM enables 4D in vivo lifetime imaging of intact and injured zebrafish and mouse brains. Optica 8(6):885–897. https://doi.org/10.1364/OPTICA.426870
117. Diaspro A, Chirico G, Collini M (2005) Two-photon fluorescence excitation and related techniques in biological microscopy. Q Rev Biophys 38(2):97–166. https://doi.org/10.1017/S0033583505004129
118. Wang T, Xu C (2020) Three-photon neuronal imaging in deep mouse brain. Optica 7(8):947. https://doi.org/10.1364/optica.395825
119. Xu C, Wise FW (2013) Recent advances in fibre lasers for nonlinear microscopy. Nat Photonics 7(11):875–882. https://doi.org/10.1038/nphoton.2013.284
120. Yew EYS, Choi H, Kim D, So PTC (2011) Wide-field two-photon microscopy with temporal focusing and HiLo background rejection. Multiphot Microsc Biomed Sci XI 7903:79031O. https://doi.org/10.1117/12.876068
121. Hwang JY et al (2011) Multimodal wide-field two-photon excitation imaging: characterization of the technique for in vivo applications. Biomed Opt Express 2(2):356. https://doi.org/10.1364/boe.2.000356
122. Escobet-Montalbán A et al (2018) Wide-field multiphoton imaging through scattering media without correction. Sci Adv 4(10):eaau1338. https://doi.org/10.1126/sciadv.aau1338
123. Macias-Romero C, Zubkovs V, Wang S, Roke S (2016) Wide-field medium-repetition-rate multiphoton microscopy reduces photodamage of living cells. Biomed Opt Express 7(4):1458. https://doi.org/10.1364/boe.7.001458
124. Palero J, Santos SICO, Artigas D, Loza-Alvarez P (2010) A simple scanless two-photon fluorescence microscope using selective plane illumination. Opt Express 18(8):8491. https://doi.org/10.1364/oe.18.008491

125. Lavagnino Z, Cella Zanacchi F, Ronzitti E, Diaspro A (2013) Two-photon excitation selective plane illumination microscopy (2PE-SPIM) of highly scattering samples: characterization and application. Opt Express 21(5):5998. https://doi.org/10.1364/oe.21.005998
126. Truong TV, Supatto W, Koos DS, Choi JM, Fraser SE (2011) Deep and fast live imaging with two-photon scanned light-sheet microscopy. Nat Methods 8(9):757–760. https://doi.org/10.1038/nmeth.1652
127. Zhang Y, Zhou T, Hu X, Xie H, Dai Q, Kong L (2019) Enhance imaging depth in wide-field two-photon microscopy by extended detection and computational reconstruction. Opt InfoBase Conf Pap Part F134(15):20117–20132. https://doi.org/10.1364/nlo.2019.ntu1b.1
128. Rosenegger DG, Tran CHT, LeDue J, Zhou N, Gordon GR (2014) A high performance, cost-effective, open-source microscope for scanning two-photon microscopy that is modular and readily adaptable. PLoS One 9(10). https://doi.org/10.1371/journal.pone.0110475
129. Bumstead JR (2018) Designing a large field-of-view two-photon microscope using optical invariant analysis. Neurophotonics 5(02):1. https://doi.org/10.1117/1.nph.5.2.025001
130. Cao R, Wallrabe HK, Periasamy A (2020) Multiphoton FLIM imaging of NAD(P)H and FAD with one excitation wavelength. J Biomed Opt 25(01):1. https://doi.org/10.1117/1.jbo.25.1.014510
131. Bower AJ, Li J, Chaney EJ, Marjanovic M, Spillman DR, Boppart SA (2018) High-speed imaging of transient metabolic dynamics using two-photon fluorescence lifetime imaging microscopy. Optica 5(10):1290. https://doi.org/10.1364/optica.5.001290
132. Jyothikumar V, Sun Y, Periasamy A (2013) Investigation of tryptophan–NADH interactions in live human cells using three-photon fluorescence lifetime imaging and Förster resonance energy transfer microscopy. J Biomed Opt 18(6):060501. https://doi.org/10.1117/1.jbo.18.6.060501
133. Shen B et al (2020) Label-free whole-colony imaging and metabolic analysis of metastatic pancreatic cancer by an autoregulating flexible optical system. Theranostics 10(4):1849–1860. https://doi.org/10.7150/thno.40869
134. Masters BR (2020) Masters BR (ed) Richard Zsigmondy and Henry Siedentopf's Ultramicroscope BT – superresolution optical microscopy: the quest for enhanced resolution and contrast. Springer, Cham, pp 165–172
135. Huisken J, Swoger J, Del Bene F, Wittbrodt J, Stelzer EHK (2004) Optical sectioning deep inside live embryos by selective plane illumination microscopy. Science 305(5686):1007–1009. https://doi.org/10.1126/science.1100035
136. Stelzer EHK (2015) Light-sheet fluorescence microscopy for quantitative biology. Nat Methods 12(1):23–26. https://doi.org/10.1038/nmeth.3219
137. Wan Y, McDole K, Keller PJ (2019) Light-sheet microscopy and its potential for understanding developmental processes. Annu Rev Cell Dev Biol 35:655–681. https://doi.org/10.1146/annurev-cellbio-100818-125311
138. Stelzer EHK et al (2021) Light sheet fluorescence microscopy. Nat Rev Methods Prim 1(1). https://doi.org/10.1038/s43586-021-00069-4
139. Saghafi S, Becker K, Hahn C, Dodt HU (2014) 3D-ultramicroscopy utilizing aspheric optics. J Biophotonics 7(1–2):117–125. https://doi.org/10.1002/jbio.201300048
140. Li H, Wu Z, Yang Z, Zhanghao K, Xi P, Jin D (2021) Axially overlapped multi-focus light sheet with enlarged field of view. Appl Phys Lett 118(22). https://doi.org/10.1063/5.0049013
141. Krzic U, Gunther S, Saunders TE, Streichan SJ, Hufnagel L (2012) Multiview light-sheet microscope for rapid in toto imaging. Nat Methods 9(7):730–733. https://doi.org/10.1038/nmeth.2064
142. Aakhte M, Müller H-AJ (2021) Multiview tiling light sheet microscopy for 3D high-resolution live imaging. Development 148(18). https://doi.org/10.1242/dev.199725
143. Meddens MBM, Liu S, Finnegan PS, Edwards TL, James CD, Lidke KA (2016) Single objective light-sheet microscopy for high-speed whole-cell 3D super-resolution. Biomed Opt Express 7(6):2219. https://doi.org/10.1364/boe.7.002219

144. Ponjavic A, Ye Y, Laue E, Lee SF, Klenerman D (2018) Sensitive light-sheet microscopy in multiwell plates using an AFM cantilever. Biomed Opt Express 9(12):5863. https://doi.org/10.1364/boe.9.005863
145. Kumar M, Kishore S, McLean DL, Kozorovitskiy Y (2021) Crossbill: an open access single objective light-sheet microscopy platform. bioRxiv. https://doi.org/10.1101/2021.04.30.442190
146. Galland R, Grenci G, Aravind A, Viasnoff V, Studer V, Sibarita J-B (2015) 3D high- and super-resolution imaging using single-objective SPIM. Nat Methods 12(7):641–644. https://doi.org/10.1038/nmeth.3402
147. Dodt H-U et al (2015) Ultramicroscopy: development and outlook. Neurophotonics 2(4):041407. https://doi.org/10.1117/1.nph.2.4.041407
148. Chen BC et al (2014) Lattice light-sheet microscopy: imaging molecules to embryos at high spatiotemporal resolution. Science 346(6208). https://doi.org/10.1126/science.1257998
149. Planchon TA et al (2011) Rapid three-dimensional isotropic imaging of living cells using Bessel beam plane illumination. Nat Methods 8(5):417–423. https://doi.org/10.1038/nmeth.1586
150. Keller PJ, Schmidt AD, Wittbrodt J, Stelzer EHK (2008) Reconstruction of zebrafish early embryonic development by scanned light sheet microscopy. Science 322(5904):1065–1069. https://doi.org/10.1126/science.1162493
151. Ren YX et al (2020) Parallelized volumetric fluorescence microscopy with a reconfigurable coded incoherent light-sheet array. Light Sci Appl 9(1). https://doi.org/10.1038/s41377-020-0245-8
152. Hofmann M, Ghebjagh SG, Lemke K, Sinzinger S (2021) Multi-sheet excitation and imaging of flow driven samples in an LSFM with a modified multi-focal diffractive lens. Opt InfoBase Conf Pap 2021:7–8. https://doi.org/10.1364/cosi.2021.cm1a.7
153. Zunino A et al (2021) Multi-plane encoded light-sheet microscopy with acousto-optics. Proc SPIE 11654
154. Axelrod D (1981) Cell-substrate contacts illuminated by total internal reflection fluorescence. J Cell Biol 89(1):141–145. https://doi.org/10.1083/jcb.89.1.141
155. Schneckenburger H (2005) Total internal reflection fluorescence microscopy: technical innovations and novel applications. Curr Opin Biotechnol 16(1):13–18. https://doi.org/10.1016/j.copbio.2004.12.004
156. Puttrich V, Rohlena J, Braun M, Lansky Z (2022) In vitro reconstitution of molecular motor-driven mitochondrial transport. Methods Mol Biol 2431:533–546. https://doi.org/10.1007/978-1-0716-1990-2_28
157. Woodward X, Stimpson EE, Kelly CV (2018) Single-lipid tracking on nanoscale membrane buds: the effects of curvature on lipid diffusion and sorting. Biochim Biophys Acta Biomembr 1860(10):2064–2075. https://doi.org/10.1016/j.bbamem.2018.05.009
158. Tannert A, Voigt P, Burgold S, Tannert S, Schaefer M (2008) Signal amplification between Gβγ release and PI3Kγ-mediated PI(3,4,5)P3 formation monitored by a fluorescent Gβγ biosensor protein and repetitive two component total internal reflection/fluorescence redistribution after photobleaching analysis. Biochemistry 47(43):11239–11250. https://doi.org/10.1021/bi800596b
159. Ruckstuhl T, Seeger S (2004) Attoliter detection volumes by confocal total-internal-reflection fluorescence microscopy. Opt Lett 29(6):569–571. https://doi.org/10.1364/OL.29.000569
160. Tokunaga M, Imamoto N, Sakata-Sogawa K (2008) Highly inclined thin illumination enables clear single-molecule imaging in cells. Nat Methods 5(2):159–161. https://doi.org/10.1038/nmeth1171
161. van't Hoff M, de Sars V, Oheim M (2008) A programmable light engine for quantitative single molecule TIRF and HILO imaging. Opt Express 16(22):18495–18504. https://doi.org/10.1364/OE.16.018495
162. Enderlein J, Ruckstuhl T, Seeger S (1999) Highly efficient optical detection of surface-generated fluorescence. Appl Optics 38(4):724–732. https://doi.org/10.1364/AO.38.000724

163. Ruckstuhl T, Verdes D, Winterflood CM, Seeger S (2011) Simultaneous near-field and far-field fluorescence microscopy of single molecules. Opt Express 19(7):6836. https://doi.org/10.1364/oe.19.006836
164. Winterflood CM, Ruckstuhl T, Reynolds NP, Seeger S (2012) Tackling sample-related artifacts in membrane FCS using parallel SAF and UAF detection. ChemPhysChem 13(16):3655–3660. https://doi.org/10.1002/cphc.201200395
165. Ries J, Ruckstuhl T, Verdes D, Schwille P (2008) Supercritical angle fluorescence correlation spectroscopy. Biophys J 94(1):221–229. https://doi.org/10.1529/biophysj.107.115998
166. Langhorst MF, Schaffer J, Goetze B (2009) Structure brings clarity: structured illumination microscopy in cell biology. Biotechnol J 4(6):858–865. https://doi.org/10.1002/biot.200900025
167. Wilson T, Juškaitis R, Neil MAA, Kozubek M (1996) Confocal microscopy by aperture correlation. Opt Lett 21(23):1879–1881. https://doi.org/10.1364/OL.21.001879
168. Sticker M, Elsässer R, Neumann M, Wolff H (2020) How to get better fluorescence images with your widefield microscope: a methodology review. Micros Today 28(6):36–43. https://doi.org/10.1017/s155192952000156x
169. Russ JC, Neal FB (2018) The image processing handbook. CRC Press
170. Agard DA (1984) Optical sectioning microscopy: cellular architecture in three dimensions. Annu Rev Biophys Bioeng 13(1):191–219. https://doi.org/10.1146/annurev.bb.13.060184.001203
171. Cox G, Sheppard C (1993) Effects of image deconvolution on optical sectioning in conventional and confocal microscopes. Bioimaging 1(2):82–95. https://doi.org/10.1002/1361-6374(199306)1:2<82::AID-BIO3>3.3.CO;2-K
172. Manz W, Arp G, Schumann-Kindel G, Szewzyk U, Reitner J (2000) Widefield deconvolution epifluorescence microscopy combined with fluorescence in situ hybridization reveals the spatial arrangement of bacteria in sponge tissue. J Microbiol Methods 40(2):125–134. https://doi.org/10.1016/S0167-7012(99)00103-7
173. Hell SW, Wichmann J (1994) Breaking the diffraction resolution limit by stimulated emission: stimulated-emission-depletion fluorescence microscopy. Opt Lett 19(11):780–782. https://doi.org/10.1364/OL.19.000780
174. Gustafsson MGL (2000) Surpassing the lateral resolution limit by a factor of two using structured illumination microscopy. J Microsc 198(2):82–87. https://doi.org/10.1046/j.1365-2818.2000.00710.x
175. Rust MJ, Bates M, Zhuang X (2006) Sub-diffraction-limit imaging by stochastic optical reconstruction microscopy (STORM). Nat Methods 3(10):793–795. https://doi.org/10.1038/nmeth929
176. Betzig E et al (2006) Imaging intracellular fluorescent proteins at nanometer resolution. Science 313(5793):1642–1645. https://doi.org/10.1126/science.1127344
177. Heintzmann R, Cremer CG (1999) Laterally modulated excitation microscopy: improvement of resolution by using a diffraction grating:185–196. https://doi.org/10.1117/12.336833
178. Heilemann M, Van De Linde S, Mukherjee A, Sauer M (2009) Super-resolution imaging with small organic fluorophores. Angew Chem Int Ed 48(37):6903–6908. https://doi.org/10.1002/anie.200902073
179. Heilemann M et al (2002) High-resolution colocalization of single dye molecules by fluorescence lifetime imaging microscopy. Anal Chem 74(14):3511–3517. https://doi.org/10.1021/ac025576g
180. Lidke K, Rieger B, Jovin T, Heintzmann R (2005) Superresolution by localization of quantum dots using blinking statistics. Opt Express 13(18):7052–7062. https://doi.org/10.1364/OPEX.13.007052
181. Sharonov A, Hochstrasser RM (2006) Wide-field subdiffraction imaging by accumulated binding of diffusing probes. Proc Natl Acad Sci U S A 103(50):18911–18916. https://doi.org/10.1073/pnas.0609643104

182. Valli J, Garcia-Burgos A, Rooney LM, de Melo e Oliveira BV, Duncan RR, Rickman C (2021) Seeing beyond the limit: a guide to choosing the right super-resolution microscopy technique. J Biol Chem 297(1). https://doi.org/10.1016/j.jbc.2021.100791
183. Liu S, Hoess P, Ries J (2022) Super-resolution microscopy for structural cell biology. Annu Rev Biophys 51(1):301–326. https://doi.org/10.1146/annurev-biophys-102521-112912
184. Prakash K, Diederich B, Heintzmann R, Schermelleh L (2022) Super-resolution microscopy: a brief history and new avenues. Philos Trans R Soc A Math Phys Eng Sci 380(2220). https://doi.org/10.1098/rsta.2021.0110
185. Eggeling C, Willig KI, Sahl SJ, Hell SW (2015) Lens-based fluorescence nanoscopy. Q Rev Biophys 48(2):178–243. https://doi.org/10.1017/S0033583514000146
186. Jacquemet G, Carisey AF, Hamidi H, Henriques R, Leterrier C (2020) The cell biologist's guide to super-resolution microscopy. J Cell Sci 133(11):jcs240713. https://doi.org/10.1242/jcs.240713
187. Long BR, Robinson DC, Zhong H (2014) Subdiffractive microscopy: techniques, applications, and challenges background: diffraction limit in biological imaging. Wiley Interdiscip Rev Syst Biol Med 6(2):151–168. https://doi.org/10.1002/wsbm.1259.Subdiffractive
188. Humpolíčková J, Benda A, Macháň R, Enderlein J, Hof M (2010) Dynamic saturation optical microscopy: employing dark-state formation kinetics for resolution enhancement. Phys Chem Chem Phys 12(39). https://doi.org/10.1039/c0cp00059k
189. Zhang Y et al (2018) Super-resolution fluorescence microscopy by stepwise optical saturation. Biomed Opt Express 9(4):1613. https://doi.org/10.1364/boe.9.001613
190. Gustafsson MGL (2005) Nonlinear structured-illumination microscopy: wide-field fluorescence imaging with theoretically unlimited resolution. Proc Natl Acad Sci U S A 102(37):13081–13086. https://doi.org/10.1073/pnas.0406877102
191. Lelek M et al (2021) Single-molecule localization microscopy. Nat Rev Methods Prim 1(1):39. https://doi.org/10.1038/s43586-021-00038-x
192. Yu J-Y, Becker SR, Folberth J, Wallin BF, Chen S, Cogswell CJ (2018) Achieving superresolution with illumination-enhanced sparsity. Opt Express 26(8):9850. https://doi.org/10.1364/oe.26.009850
193. Opstad IS et al (2020) Fluorescence fluctuations-based super-resolution microscopy techniques: an experimental comparative study
194. Mukamel EA, Babcock H, Zhuang X (2012) Statistical deconvolution for superresolution fluorescence microscopy. Biophys J 102(10):2391–2400. https://doi.org/10.1016/j.bpj.2012.03.070
195. Manton JD, Xiao Y, Turner RD, Christie G, Rees EJ (2018) ELM: super-resolution analysis of wide-field images of fluorescent shell structures. Methods Appl Fluoresc 6(3). https://doi.org/10.1088/2050-6120/aac28e
196. Enderle T, Ha T, Chemla DS, Weiss S (1998) Near-field fluorescence microscopy of cells. Ultramicroscopy 71(1–4):303–309. https://doi.org/10.1016/s0304-3991(97)00075-2
197. Enderle T, Ha T, Ogletree DF, Chemla DS, Magowan C, Weiss S (1997) Membrane specific mapping and colocalization of malarial and host skeletal proteins in the plasmodium falciparum infected erythrocyte by dual-color near-field scanning optical microscopy. Proc Natl Acad Sci U S A 94(2):520–525. https://doi.org/10.1073/pnas.94.2.520
198. García-Parajó MF et al (2005) Near-field fluorescence microscopy. NanoBiotechnology 1(1):113–120. https://doi.org/10.1385/NBT:1:1:113
199. Harootunian A, Betzig E, Isaacson M, Lewis A (1986) Super-resolution fluorescence near-field scanning optical microscopy. Appl Phys Lett 49(11):674–676. https://doi.org/10.1063/1.97565
200. Schwartz O, Oron D (2012) Improved resolution in fluorescence microscopy using quantum correlations. Phys Rev A 85(3):1–5. https://doi.org/10.1103/PhysRevA.85.033812
201. Schwartz O, Levitt JM, Tenne R, Itzhakov S, Deutsch Z, Oron D (2013) Superresolution microscopy with quantum emitters. Nano Lett 13(12):5832–5836. https://doi.org/10.1021/nl402552m

202. Tenne R et al (2019) Super-resolution enhancement by quantum image scanning microscopy. Nat Photonics 13(2):116–122. https://doi.org/10.1038/s41566-018-0324-z
203. Israel Y, Tenne R, Oron D, Silberberg Y (2017) Quantum correlation enhanced super-resolution localization microscopy enabled by a fibre bundle camera. Nat Commun 8:1–5. https://doi.org/10.1038/ncomms14786
204. Classen A, von Zanthier J, Scully MO, Agarwal GS (2017) Superresolution via structured illumination quantum correlation microscopy. Optica 4(6):580. https://doi.org/10.1364/optica.4.000580
205. Korobchevskaya K et al (2016) Intensity weighted subtraction microscopy approach for image contrast and resolution enhancement. Sci Rep 6(April). https://doi.org/10.1038/srep25816
206. Hell SW, Kroug M (1995) Ground-state-depletion fluorscence microscopy: a concept for breaking the diffraction resolution limit. Appl Phys B Lasers Opt 60(5):495–497. https://doi.org/10.1007/BF01081333
207. Eilers Y, Ta H, Gwosch KC, Balzarotti F, Hell SW (2018) MINFLUX monitors rapid molecular jumps with superior spatiotemporal resolution. Proc Natl Acad Sci 115(24). https://doi.org/10.1073/pnas.1801672115
208. Friedrich M, Gan Q, Ermolayev V, Harms GS (2011) STED-SPIM: stimulated emission depletion improves sheet illumination microscopy resolution. Biophys J 100(8):L43–L45. https://doi.org/10.1016/j.bpj.2010.12.3748
209. Prakash K (2021) Laser-free super-resolution microscopy. Philos Trans R Soc A Math Phys Eng Sci 379(2199):20200144. https://doi.org/10.1098/rsta.2020.0144
210. Mao H et al (2019) Cost-efficient nanoscopy reveals nanoscale architecture of liver cells and platelets. Nanophotonics. https://doi.org/10.1515/nanoph-2019-0066
211. Hosny NA, Song M, Connelly JT, Ameer-Beg S, Knight MM, Wheeler AP (2013) Super-resolution imaging strategies for cell biologists using a spinning disk microscope. PLoS One 8(10). https://doi.org/10.1371/journal.pone.0074604
212. Gustavsson A-K, Petrov PN, Lee MY, Shechtman Y, Moerner WE (2018) 3D single-molecule super-resolution microscopy with a tilted light sheet. Nat Commun 9(1). https://doi.org/10.1038/s41467-017-02563-4
213. Lu C-H et al (2019) Lightsheet localization microscopy enables fast, large-scale, and three-dimensional super-resolution imaging. Commun Biol 2(1):177. https://doi.org/10.1038/s42003-019-0403-9
214. Thompson RE, Larson DR, Webb WW (2002) Precise nanometer localization analysis for individual fluorescent probes. Biophys J 82(5):2775–2783. https://doi.org/10.1016/S0006-3495(02)75618-X
215. Yildiz A, Selvin PR (2005) Fluorescence imaging with one nanometer accuracy: application to molecular motors. Acc Chem Res 38(7):574–582. https://doi.org/10.1021/ar040136s
216. Weisenburger S et al (2017) Cryogenic optical localization provides 3D protein structure data with angstrom resolution. Nat Methods 14(2):141–144. https://doi.org/10.1038/nmeth.4141
217. Hess ST, Girirajan TPK, Mason MD (2006) Ultra-high resolution imaging by fluorescence photoactivation localization microscopy. Biophys J 91(11):4258–4272. https://doi.org/10.1529/biophysj.106.091116
218. Lippincott-Schwartz J, Patterson GH (2009) Photoactivatable fluorescent proteins for diffraction-limited and super-resolution imaging. Trends Cell Biol 19(11):555–565. https://doi.org/10.1016/j.tcb.2009.09.003
219. Shcherbakova DM, Sengupta P, Lippincott-Schwartz J, Verkhusha VV (2014) Photocontrollable fluorescent proteins for superresolution imaging. Annu Rev Biophys 43:303–329. https://doi.org/10.1146/annurev-biophys-051013-022836
220. Wang S, Moffitt JR, Dempsey GT, Xie XS, Zhuang X (2014) Characterization and development of photoactivatable fluorescent proteins for single-molecule-based superresolution imaging. Proc Natl Acad Sci U S A 111(23):8452–8457. https://doi.org/10.1073/pnas.1406593111
221. van de Linde S et al (2011) Direct stochastic optical reconstruction microscopy with standard fluorescent probes. Nat Protoc 6(7):991–1009. https://doi.org/10.1038/nprot.2011.336

222. Dempsey GT, Vaughan JC, Chen KH, Bates M, Zhuang X (2011) Evaluation of fluorophores for optimal performance in localization-based super-resolution imaging. Nat Methods 8(12): 1027–1036. https://doi.org/10.1038/nmeth.1768
223. Vogelsang J et al (2008) A reducing and oxidizing system minimizes photobleaching and blinking of fluorescent dyes. Angew Chem Int Ed 47(29):5465–5469. https://doi.org/10.1002/anie.200801518
224. Jungmann R, Avendaño MS, Woehrstein JB, Dai M, Shih WM, Yin P (2014) Multiplexed 3D cellular super-resolution imaging with DNA-PAINT and exchange-PAINT. Nat Methods 11(3):313–318. https://doi.org/10.1038/nmeth.2835
225. Schoen I, Ries J, Klotzsch E, Ewers H, Vogel V (2011) Binding-activated localization microscopy of DNA l. Nano Lett 11(9):4008–4011. https://doi.org/10.1021/nl2025954
226. Kuo C, Hochstrasser RM (2011) Super-resolution microscopy of lipid bilayer phases. J Am Chem Soc 133(13):4664–4667. https://doi.org/10.1021/ja1099193
227. Manley S et al (2008) High-density mapping of single-molecule trajectories with photoactivated localization microscopy. Nat Methods 5(2):155–157. https://doi.org/10.1038/nmeth.1176
228. Rossier O et al (2012) Integrins β1 and β3 exhibit distinct dynamic nanoscale organizations inside focal adhesions. Nat Cell Biol 14(10):1057–1067. https://doi.org/10.1038/ncb2588
229. Gao Y, Foo YH, Winardhi R, Tang Q, Yan J, Kenney L (2017) Charged residues in the H-NS linker drive DNA binding and gene silencing in single cells. Proc Natl Acad Sci 114: 201716721. https://doi.org/10.1073/pnas.1716721114
230. Kapanidis A, Uphoff S, Stracy M (2018) Understanding protein mobility in bacteria by tracking single molecules. J Mol Biol 430. https://doi.org/10.1016/j.jmb.2018.05.002
231. Ovesný M, Křížek P, Borkovec J, Švindrych Z, Hagen GM (2014) ThunderSTORM: a comprehensive ImageJ plug-in for PALM and STORM data analysis and super-resolution imaging. Bioinformatics 30(16). https://doi.org/10.1093/bioinformatics/btu202
232. Palayret M et al (2015) Virtual-'light-sheet' single-molecule localisation microscopy enables quantitative optical sectioning for super-resolution imaging. PLoS One 10(4):1–15. https://doi.org/10.1371/journal.pone.0125438
233. von Diezmann L, Shechtman Y, Moerner WE (2017) Three-dimensional localization of single molecules for super-resolution imaging and single-particle tracking. Chem Rev 117(11): 7244–7275. https://doi.org/10.1021/acs.chemrev.6b00629
234. Bon P et al (2018) Self-interference 3D super-resolution microscopy for deep tissue investigations. Nat Methods 15(6):449–454. https://doi.org/10.1038/s41592-018-0005-3
235. Rehman SA, Carr AR, Lenz MO, Lee SF, O'Holleran K (2018) Maximizing the field of view and accuracy in 3D single molecule localization microscopy. Opt Express 26(4). https://doi.org/10.1364/OE.26.004631
236. Wang W et al (2019) Generalized method to design phase masks for 3D super-resolution microscopy. Opt Express 27(3):3799. https://doi.org/10.1364/oe.27.003799
237. Hajj B et al (2014) Whole-cell, multicolor superresolution imaging using volumetric multifocus microscopy. Proc Natl Acad Sci U S A 111(49):17480–17485. https://doi.org/10.1073/pnas.1412396111
238. Oudjedi L et al (2016) Astigmatic multifocus microscopy enables deep 3D super-resolved imaging. Biomed Opt Express 7(6). https://doi.org/10.1364/BOE.7.002163
239. Sims RR et al (2020) Single molecule light field microscopy. Optica 7(9):1065. https://doi.org/10.1364/optica.397172
240. Shtengel G et al (2009) Interferometric fluorescent super-resolution microscopy resolves 3D cellular ultrastructure understanding molecular-scale architecture of cells requires determination of 3D locations of specific proteins with accuracy match-ing their nanometer-length sca. Proc Natl Acad Sci 106(9):3125–3130
241. Shroff H, Galbraith CG, Galbraith JA, Betzig E (2008) Live-cell photoactivated localization microscopy of nanoscale adhesion dynamics. Nat Methods 5(5):417–423. https://doi.org/10.1038/nmeth.1202

242. Holden SJ, Uphoff S, Kapanidis AN (2011) DAOSTORM: an algorithm for high-density super-resolution microscopy. Nat Methods 8(4):279–280. https://doi.org/10.1038/nmeth0411-279
243. Min J et al (2014) FALCON: fast and unbiased reconstruction of high-density super-resolution microscopy data. Sci Rep 4:4577. https://doi.org/10.1038/srep04577
244. Hugelier S et al (2016) Sparse deconvolution of high-density super-resolution images. Sci Rep 6. https://doi.org/10.1038/srep21413
245. Dertinger T, Colyer R, Iyer G, Weiss S, Enderlein J (2009) Fast, background-free, 3D super-resolution optical fluctuation imaging (SOFI). Proc Natl Acad Sci U S A 106(52):22287–22292. https://doi.org/10.1073/pnas.0907866106
246. Dertinger T, Pallaoro A, Braun G, Ly S, Laurence TA, Weiss S (2013) Advances in superresolution optical fluctuation imaging (SOFI). Q Rev Biophys 46(2):210–221. https://doi.org/10.1017/S0033583513000036
247. Geissbuehler S, Bocchio NL, Dellagiacoma C, Berclaz C, Leutenegger M, Lasser T (2012) Mapping molecular statistics with balanced super-resolution optical fluctuation imaging (bSOFI). Opt Nanoscopy 1(1):4. https://doi.org/10.1186/2192-2853-1-4
248. Agarwal K, Macháň R (2016) Multiple signal classification algorithm for super-resolution fluorescence microscopy. Nat Commun 7:13752. https://doi.org/10.1038/ncomms13752
249. Deng Y, Sun M, Lin PH, Ma J, Shaevitz JW (2014) Spatial covariance reconstructive (SCORE) super-resolution fluorescence microscopy. PLoS One 9(4):1–9. https://doi.org/10.1371/journal.pone.0094807
250. Yahiatene I, Hennig S, Müller M, Huser T (2015) Entropy-based super-resolution imaging (ESI): from disorder to fine detail. ACS Photonics 2(8):1049–1056. https://doi.org/10.1021/acsphotonics.5b00307
251. Cox S et al (2011) Bayesian localization microscopy reveals nanoscale podosome dynamics. Nat Methods 9(2):195–200. https://doi.org/10.1038/nmeth.1812
252. Gong H, Guo W, Neil MAA (2021) GPU-accelerated real-time reconstruction in python of three-dimensional datasets from structured illumination microscopy with hexagonal patterns. Philos Trans R Soc A Math Phys Eng Sci 379(2199). https://doi.org/10.1098/rsta.2020.0162
253. Christensen CN, Ward EN, Lu M, Lio P, Kaminski CF (2021) ML-SIM: universal reconstruction of structured illumination microscopy images using transfer learning. Biomed Opt Express 12(5):2720–2733. https://doi.org/10.1364/BOE.414680
254. Abrahamsson S et al (2017) Multifocus structured illumination microscopy for fast volumetric super-resolution imaging. Biomed Opt Express 8(9):4135. https://doi.org/10.1364/boe.8.004135
255. Chang B-J, Perez Meza VD, Stelzer EHK (2017) csiLSFM combines light-sheet fluorescence microscopy and coherent structured illumination for a lateral resolution below 100 nm. Proc Natl Acad Sci 114(19). https://doi.org/10.1073/pnas.1609278114
256. Ströhl F, Kaminski CF (2019) A concept for single-shot volumetric fluorescence imaging via orthogonally polarized excitation lattices. Sci Rep 9(1):1–9. https://doi.org/10.1038/s41598-019-42743-4
257. Yeh L-H, Tian L, Waller L (2016) Structured illumination microscopy with unknown patterns and a statistical prior. https://doi.org/10.1364/BOE.8.000695
258. Christensen CN, Ward EN, Lio P, Kaminski CF (2020) ML-SIM: a deep neural network for reconstruction of structured illumination microscopy images, pp 1–9
259. Mudry E et al (2012) Structured illumination microscopy using unknown speckle patterns. Nat Photonics 6(5):312–315. https://doi.org/10.1038/nphoton.2012.83
260. Lukeš T et al (2014) Three-dimensional super-resolution structured illumination microscopy with maximum a posteriori probability image estimation. Opt Express 22(24):29805. https://doi.org/10.1364/oe.22.029805
261. Min J et al (2013) Fluorescent microscopy beyond diffraction limits using speckle illumination and joint support recovery. Sci Rep 3:1–6. https://doi.org/10.1038/srep02075

262. Jost A, Tolstik E, Feldmann P, Wicker K, Sentenac A, Heintzmann R (2015) Optical sectioning and high resolution in single-slice structured illumination microscopy by thick slice blind-SIM reconstruction. PLoS One 10(7). https://doi.org/10.1371/journal.pone.0132174
263. Chakrova N, Heintzmann R, Rieger B, Stallinga S (2015) Studying different illumination patterns for resolution improvement in fluorescence microscopy. Opt Express 23(24):31367. https://doi.org/10.1364/oe.23.031367
264. Lu-Walther HW et al (2016) Nonlinear structured illumination using a fluorescent protein activating at the readout wavelength. PLoS One 11(10):1–14. https://doi.org/10.1371/journal.pone.0165148
265. Zhang H, Zhao M, Peng L (2011) Nonlinear structured illumination microscopy by surface plasmon enhanced stimulated emission depletion. Opt Express 19(24):24783. https://doi.org/10.1364/oe.19.024783
266. Joseph J, Faiz KP, Lahrberg M, Tinguely JC, Ahluwalia BS (2020) Improving the space-bandwidth product of structured illumination microscopy using a transillumination configuration. J Phys D Appl Phys 53(4). https://doi.org/10.1088/1361-6463/ab4e68
267. Yilmaz H, van Putten EG, Bertolotti J, Lagendijk A, Vos WL, Mosk AP (2015) Speckle correlation resolution enhancement of wide-field fluorescence imaging. Optica 2(5):424. https://doi.org/10.1364/optica.2.000424
268. Cragg GE, So PTC (2000) Lateral resolution enhancement with standing evanescent waves. Opt Lett 25(1):46. https://doi.org/10.1364/ol.25.000046
269. Helle ØI, Dullo FT, Lahrberg M, Tinguely JC, Hellesø OG, Ahluwalia BS (2020) Structured illumination microscopy using a photonic chip. Nat Photonics 14(7):431–438. https://doi.org/10.1038/s41566-020-0620-2
270. Tang M et al (2022) High-refractive-index chip with periodically fine-tuning gratings for tunable virtual-Wavevector spatial frequency shift universal super-resolution imaging. Adv Sci 9(9):1–11. https://doi.org/10.1002/advs.202103835
271. Lee YU et al (2021) Metamaterial assisted illumination nanoscopy via random super-resolution speckles. Nat Commun 12(1). https://doi.org/10.1038/s41467-021-21835-8
272. Lee YU et al (2021) Organic hyperbolic material assisted illumination nanoscopy. Adv Sci 8(22):1–7. https://doi.org/10.1002/advs.202102230
273. Ponsetto JL et al (2017) Experimental demonstration of localized plasmonic structured illumination microscopy. ACS Nano 11(6):5344–5350. https://doi.org/10.1021/acsnano.7b01158
274. Wei F, Liu Z (2010) Plasmonic structured illumination microscopy. Nano Lett 10(7):2531–2536. https://doi.org/10.1021/nl1011068
275. Bertero M, Boccacci P, Defrise M, De Mol C, Pike ER (1989) Super-resolution in confocal scanning microscopy: II. The incoherent case. Inverse Probl 5(4):441–461. https://doi.org/10.1088/0266-5611/5/4/003
276. Müller CB, Enderlein J (2010) Image scanning microscopy. Phys Rev Lett 104(19):1–4. https://doi.org/10.1103/PhysRevLett.104.198101
277. Sheppard CJR, Mehta SB, Heintzmann R (2013) Superresolution by image scanning microscopy using pixel reassignment. Opt Lett 38(15):2889. https://doi.org/10.1364/ol.38.002889
278. Schulz O et al (2013) Resolution doubling in fluorescence microscopy with confocal spinning-disk image scanning microscopy. Proc Natl Acad Sci U S A 110(52):21000–21005. https://doi.org/10.1073/pnas.1315858110
279. Sheppard C (1988) Super-resolution in confocal imaging. Opt Int J Light Electron Opt 80:53
280. Sheppard CJR, Castello M, Tortarolo G, Vicidomini G, Diaspro A (2017) Image formation in image scanning microscopy, including the case of two-photon excitation. J Opt Soc Am A 34(8):1339. https://doi.org/10.1364/josaa.34.001339
281. Korobchevskaya K, Lagerholm BC, Colin-York H, Fritzsche M (2017) Exploring the potential of Airyscan microscopy for live cell imaging. Photodermatol 4(3). https://doi.org/10.3390/photonics4030041

282. Gregor I, Spiecker M, Petrovsky R, Großhans J, Ros R, Enderlein J (2017) Rapid nonlinear image scanning microscopy. Nat Methods 14(11):1087–1089. https://doi.org/10.1038/nmeth.4467
283. Roth S, Sheppard CJR, Wicker K, Heintzmann R (2013) Optical photon reassignment microscopy (OPRA). Opt Nanoscopy 2(1):5. https://doi.org/10.1186/2192-2853-2-5
284. Castello M et al (2019) A robust and versatile platform for image scanning microscopy enabling super-resolution FLIM. Nat Methods 16(2):175–178. https://doi.org/10.1038/s41592-018-0291-9
285. Azuma T, Kei T (2015) Super-resolution spinning-disk confocal microscopy using optical photon reassignment. Opt Express 23(11):15003. https://doi.org/10.1364/oe.23.015003
286. York AG et al (2013) Instant super-resolution imaging in live cells and embryos via analog image processing. Nat Methods. https://doi.org/10.1038/nmeth.2687
287. Winter PW et al (2014) Two-photon instant structured illumination microscopy improves the depth penetration of super-resolution imaging in thick scattering samples. Optica 1(3):181. https://doi.org/10.1364/optica.1.000181
288. Yu J-Y, Narumanchi VV, Chen S, Xing J, Becker SR, Cogswell CJ (2020) Analyzing the super-resolution characteristics of focused-spot illumination approaches. J Biomed Opt 25(05):1. https://doi.org/10.1117/1.jbo.25.5.056501
289. Hayashi S (2016) Resolution doubling using confocal microscopy via analogy with structured illumination microscopy. Jpn J Appl Phys 55(8). https://doi.org/10.7567/JJAP.55.082501
290. Fallet C et al (2014) Conical diffraction as a versatile building block to implement new imaging modalities for superresolution in fluorescence microscopy. Nanoimaging Nanospectrosc II 9169:9–14. https://doi.org/10.1117/12.2061059
291. Fallet C et al (2015) A new method to achieve tens of nm axial super-localization based on conical diffraction PSF shaping. Single Mol Spectrosc Superresolution Imaging VIII 9331:65–75. https://doi.org/10.1117/12.2077712
292. Schrader M, Hell SW, van der Voort HTM (1996) Potential of confocal microscopes to resolve in the 50–100 nm range. Appl Phys Lett 69(24):3644–3646. https://doi.org/10.1063/1.117010
293. Weigert M et al (2018) Content-aware image restoration: pushing the limits of fluorescence microscopy. Nat Methods 15(12):1090–1097. https://doi.org/10.1038/s41592-018-0216-7
294. Culley S, Tosheva KL, Matos Pereira P, Henriques R (2018) SRRF: Universal live-cell super-resolution microscopy. Int J Biochem Cell Biol 101:74. https://doi.org/10.1016/j.biocel.2018.05.014
295. Gustafsson N, Culley S, Ashdown G, Owen DM, Pereira PM, Henriques R (2016) Fast live-cell conventional fluorophore nanoscopy with ImageJ through super-resolution radial fluctuations. Nat Commun 7:1–9. https://doi.org/10.1038/ncomms12471
296. García ET et al (2021) Nanoscopic resolution within a single imaging frame. bioRxiv:2021.10.17.464398
297. Cordelières F et al (2016) Bioimage data analysis. WILEY-VCH, Weinheim
298. Miura K, Sladoje N (2020) Bioimage data analysis workflows. Springer, Cham
299. Kurita T, Otsu N, Abdelmalek N (1992) Maximum likelihood thresholding based on population mixture models. Pattern Recogn 25(10):1231–1240. https://doi.org/10.1016/0031-3203(92)90024-D
300. Otsu N (1979) A threshold selection method from gray-level histograms. IEEE Trans Syst Man Cybern 9(1):62–66. https://doi.org/10.1109/TSMC.1979.4310076
301. Arzt M et al (2022) LABKIT: labeling and segmentation toolkit for big image data. Front Comp Sci 4. https://doi.org/10.3389/fcomp.2022.777728
302. Arganda-Carreras I et al (2017) Trainable Weka segmentation: a machine learning tool for microscopy pixel classification. Bioinformatics 33(15):2424–2426. https://doi.org/10.1093/bioinformatics/btx180
303. Krull A, Buchholz TO, Jug F (2019, 2019) Noise2void-Learning denoising from single noisy images. Proc IEEE Comput Soc Conf Comput Vis Pattern Recognit:2124–2132. https://doi.org/10.1109/CVPR.2019.00223

304. Mekhail SP, Arbuthnott G, Chormaic SN (2016) Advances in fibre microendoscopy for neuronal imaging. Opt Data Process Storage 2(1):30–42. https://doi.org/10.1515/odps-2016-0003
305. Supekar OD et al (2022) Miniature structured illumination microscope for in vivo 3D imaging of brain structures with optical sectioning. Biomed Opt Express 13(4):2530. https://doi.org/10.1364/boe.449533
306. Schmid B et al (2013) High-speed panoramic light-sheet microscopy reveals global endodermal cell dynamics. Nat Commun 4(1):2207. https://doi.org/10.1038/ncomms3207
307. Pomarico E et al (2020) Quantifying the effect of image compression on supervised learning applications in optical microscopy
308. Amat F, Höckendorf B, Wan Y, Lemon WC, McDole K, Keller PJ (2015) Efficient processing and analysis of large-scale light-sheet microscopy data. Nat Protoc 10(11):1679–1696. https://doi.org/10.1038/nprot.2015.111
309. Vopson MM (2020) The information catastrophe. AIP Adv 10(8):85014. https://doi.org/10.1063/5.0019941